



*Supplement of*

## **Modeling polar marine ecosystem functions guided by bacterial physiological and taxonomic traits**

**Hyewon Heather Kim et al.**

*Correspondence to:* Hyewon Heather Kim (hkim@whoi.edu)

The copyright of individual parts of the supplement might differ from the article licence.

## Supplementary Material

**Figure S1: Physical forcing fields for each year.** PAR: photosynthetically active radiation, MLD: mixed layer depth.

**Figure S2: Agreement between observations and model output before and after optimization for 2010-11.** Error as the difference and agreement between optimized model outputs (opt.) and model outputs before optimization (init.) for each data type for 2010-11. Model outputs and observations are normalized by the mean of optimized model outputs and observations, respectively.

**Figure S3: Agreement between observations and model output before and after optimization for 2011-12.** Error as the difference and agreement between optimized model outputs (opt.) and model outputs before optimization (init.) for each data type for 2011-12. Model outputs and observations are normalized by the mean of optimized model outputs and observations, respectively.

**Figure S4: Agreement between observations and model output before and after optimization for 2012-13.** Error as the difference and agreement between optimized model outputs (opt.) and model outputs before optimization (init.) for each data type for 2012-13. Model outputs and observations are normalized by the mean of optimized model outputs and observations, respectively.

**Figure S5: Agreement between observations and model output before and after optimization for 2013-14.** Error as the difference and agreement between optimized model outputs (opt.) and model outputs before optimization (init.) for each data type for 2013-14. Model outputs and observations are normalized by the mean of optimized model outputs and observations, respectively.

**Figure S6: Agreement between observations and model output before and after optimization for the climatological year.** Error as the difference and agreement between optimized model outputs (opt.) and model outputs before optimization (init.) for each data type for the climatological year (i.e., the climatological model). Model outputs and observations are normalized by the mean of optimized model outputs and observations, respectively.

**Figure S7: Agreement in seasonal cycles between observations and model output before and after optimization.** Obs.: observations, init.: before optimization, opt.: after optimization.

**Figure S8: Seasonal patterns of modelled bacterial C stocks and flows.** Errors as the Monte Carlo experiment-derived standard deviation. Black line: 2010-11, blue line: 2011-12, red line: 2012-13, and green line: 2013-14.

**Figure S9: Annual mean carbon stocks and flows normalized by NPP.** Carbon stocks and flows and other stocks (e.g., nutrients) averaged over the growth season in each year that are normalized by NPP (for C flows) and NPP in 1-day (for C stocks) are denoted as the numbers on the first row, while the numbers on the second row or in the parentheses are the standard deviation propagated from averaging over the growth season and the Monte Carlo experiment-derived uncertainties. Numbers around the arrows represent intercompartmental flows and do not necessarily balance to zero due to the build-up or loss in a compartment over the growth season. The magnitude of the N and P flows, as well as the flows smaller than  $0.01 \text{ mmol C m}^{-3} \text{ d}^{-1}$ , are omitted. RDOM and higher levels are implicit.

**Figure S10: Properties of the emergent self-organizing map for bacterial community structure shown as taxonomic modes (modified from Bowman et al., 2017).** Map units are colored and numbered according to taxonomic mode membership (a). Location of samples used in this study within the map (b). The map is trained with a larger set of samples, here, only those samples for which BP and flow cytometry data are available (those samples used in this study) are shown. Mode boundaries are the same as in (a). Each sample is placed within the map unit that has the most similar community structure, however, the position of each sample within the map unit is random. Relative abundance of the most abundant taxa in the microbial community structure dataset in each map unit after training (c-h). For example, *Ca. P. ubique* HTCC1062 (c) dominate samples associated with mode 6, while *Dokdonia sp.* MED134 (e) dominate samples associated with mode 7. The boundaries across all panels are as in (a).

**Figure S11: Warming alone experiments.** Seasonal progression of the modelled HNA and LNA bacterial stocks and processes and key ecosystem functions over the growth season under observed physical forcing and warming alone conditions (a) and the percent change of the corresponding variable under warming alone conditions compared to observed temperature fields (b).

**Figure S12: Melting alone experiments.** Seasonal progression of the modelled HNA and LNA bacterial stocks and processes and key ecosystem functions over the growth season under observed physical forcing and melting alone conditions (a) and the percent change of the corresponding variable under melting alone conditions compared to observed sea-ice fields (b).

**Table S1: The number of assimilated observations for each data type.** SDOC, POC, and PON data types are not assimilated for 2012-13 and 2013-14 due to the lack of observations.

**Table S2: List of model parameters for 2010-11.** Summary of the 2010-11 model parameter symbol and definition, initial guess ( $p_0$ ) and optimized values ( $p_f$ ) for optimizable parameters, the cost function gradient (sensitivity) with regard to the optimized parameter ( $\partial J/\partial p$ ), and prescribed values for fixed model parameters over the course of simulations. The parameter with ‘n/a’ in the parenthesis is an updated parameter, while the parameter with values in the parenthesis is an optimized parameter with its upper and lower bounds in the parenthesis. The uncertainties for these upper and lower bounds are calculated as:  $p_f \times e^{\pm\sigma_f}$  where  $p_f$  is the value of the optimized parameter and  $\sigma_f$  is the square roots of diagonal elements of the inverse of the Hessian matrix. The cost function gradient with regard to the optimized parameter ( $\partial J/\partial p$ ) after data assimilation defined as:  $\Delta J/e^{\Delta p}$  where  $e^{\Delta p} \approx \Delta p$  for an infinitely small  $\Delta p$ . For example, a 10% change of a parameter ( $\Delta p = 10\%$ ) leads to a total cost change equivalent to 10% of the corresponding gradient. OP: an optimized parameter with  $\sigma_f$  larger than 50%, CS: an optimized parameter with  $\sigma_f$  smaller than 50% (i.e., constrained parameters; details in Kim et al., 2021).

**Table S3: List of model parameters for 2011-12.** Summary of the 2011-12 model parameter symbol and definition, initial guess ( $p_0$ ) and optimized values ( $p_f$ ) for optimizable parameters, the cost function gradient (sensitivity) with regard to the optimized parameter ( $\partial J/\partial p$ ), and prescribed values for fixed model parameters over the course of simulations. The parameter with ‘n/a’ in the parenthesis is an updated parameter, while the parameter with values in the parenthesis is an optimized parameter with its upper and lower bounds in the parenthesis. The uncertainties for these upper and lower bounds are calculated as:  $p_f \times e^{\pm\sigma_f}$  where  $p_f$  is the value of the optimized parameter and  $\sigma_f$  is the square roots of diagonal elements of the inverse of the Hessian matrix. The cost function gradient with regard to the optimized parameter ( $\partial J/\partial p$ ) after data assimilation defined as:  $\Delta J/e^{\Delta p}$  where  $e^{\Delta p} \approx \Delta p$  for an infinitely small  $\Delta p$ . For example, a 10% change of a parameter ( $\Delta p = 10\%$ ) leads to a total cost change equivalent to 10% of the corresponding gradient. OP: an optimized parameter with  $\sigma_f$  larger than 50%, CS: an optimized parameter with  $\sigma_f$  smaller than 50% (i.e., constrained parameters; details in Kim et al., 2021).

**Table S4: List of model parameters for 2012-13.** Summary of the 2012-13 model parameter symbol and definition, initial guess ( $p_0$ ) and optimized values ( $p_f$ ) for optimizable parameters, the cost function gradient (sensitivity) with regard to the optimized parameter ( $\partial J/\partial p$ ), and prescribed values for fixed model parameters over the course of simulations. The parameter with ‘n/a’ in the parenthesis is an updated parameter, while the parameter with values in the parenthesis is an optimized parameter with its upper and lower bounds in the parenthesis. The uncertainties for these upper and lower bounds are calculated as:  $p_f \times e^{\pm\sigma_f}$  where  $p_f$  is the value of the optimized parameter and  $\sigma_f$  is the square roots of diagonal elements of the inverse of the Hessian matrix. The cost function gradient with regard to the optimized parameter ( $\partial J/\partial p$ ) after data assimilation defined as:  $\Delta J/e^{\Delta p}$  where  $e^{\Delta p} \approx \Delta p$  for an infinitely small  $\Delta p$ . For example, a 10% change of a parameter ( $\Delta p = 10\%$ ) leads to a total cost change equivalent to 10% of the corresponding gradient. OP: an optimized parameter with  $\sigma_f$  larger than 50%, CS: an optimized parameter with  $\sigma_f$  smaller than 50% (i.e., constrained parameters; details in Kim et al., 2021).

**Table S5: List of model parameters for 2013-14.** Summary of the 2013-14 model parameter symbol and definition, initial guess ( $p_0$ ) and optimized values ( $p_f$ ) for optimizable parameters, the cost function gradient (sensitivity) with regard to the optimized parameter ( $\partial J/\partial p$ ), and prescribed values for fixed model parameters over the course of simulations. The parameter with ‘n/a’ in the parenthesis is an updated parameter, while the parameter with values in the parenthesis is an optimized parameter with its upper and lower bounds in the parenthesis. The uncertainties for these upper and lower bounds are calculated as:  $p_f \times e^{\pm\sigma_f}$  where  $p_f$  is the value of the optimized parameter and  $\sigma_f$  is the square roots of diagonal elements of the inverse of the Hessian matrix. The cost function gradient with regard to the optimized parameter ( $\partial J/\partial p$ ) after data assimilation defined as:  $\Delta J/e^{\Delta p}$  where  $e^{\Delta p} \approx \Delta p$  for an infinitely small  $\Delta p$ . For example, a 10% change of a parameter ( $\Delta p = 10\%$ ) leads to a total cost change equivalent to 10% of the corresponding gradient. OP: an optimized parameter with  $\sigma_f$  larger than 50%, CS: an optimized parameter with  $\sigma_f$  smaller than 50% (i.e., constrained parameters; details in Kim et al., 2021).

**Table S6: List of model parameters for the climatological year.** Summary of the climatological model parameter symbol and definition, initial guess ( $p_0$ ) and optimized values ( $p_f$ ) for optimizable parameters, the cost function gradient with regard to the optimized parameter ( $\partial J/\partial p$ ), and prescribed values for fixed model parameters over the course of simulations. The parameter with ‘n/a’ in the parenthesis is an updated parameter, while the parameter with values in the parenthesis is an optimized parameter with its upper and lower bounds in the parenthesis. The uncertainties for these upper and lower bounds are calculated as:  $p_f \times e^{\pm\sigma_f}$  where  $p_f$  is the value of the optimized parameter and  $\sigma_f$  is the square roots of diagonal elements of the inverse of the Hessian matrix. The cost function gradient with regard to the optimized parameter ( $\partial J/\partial p$ ) after data assimilation defined as:  $\Delta J/e^{\Delta p}$  where  $e^{\Delta p} \approx \Delta p$  for an infinitely small  $\Delta p$ . For example, a 10% change of a parameter ( $\Delta p = 10\%$ ) leads to a total cost change equivalent to 10% of the corresponding gradient. OP: an optimized parameter with  $\sigma_f$  larger than 50%, CS: an optimized parameter with  $\sigma_f$  smaller than 50% (i.e., constrained parameters; details in Kim et al., 2021).

**Table S7: Interannual variability of observed and modelled ecosystem variables.** Anomalies of sea ice and temperature were specified by comparing each year’s mean to the 4-year climatology. Annual maximum and mean values calculated only at the time points where observations are available for direct model-observation comparisons. DA: diatom Chl, CR: cryptophyte Chl.

**Text S1. Model processes**

**Text S2. Physical forcing**

**Text S3. Data assimilation and parameter optimization processes**

**Text S4. Model initialization, spin-up, and boundary conditions**

**Text S5. Target error adjustment**

**Figure S1**

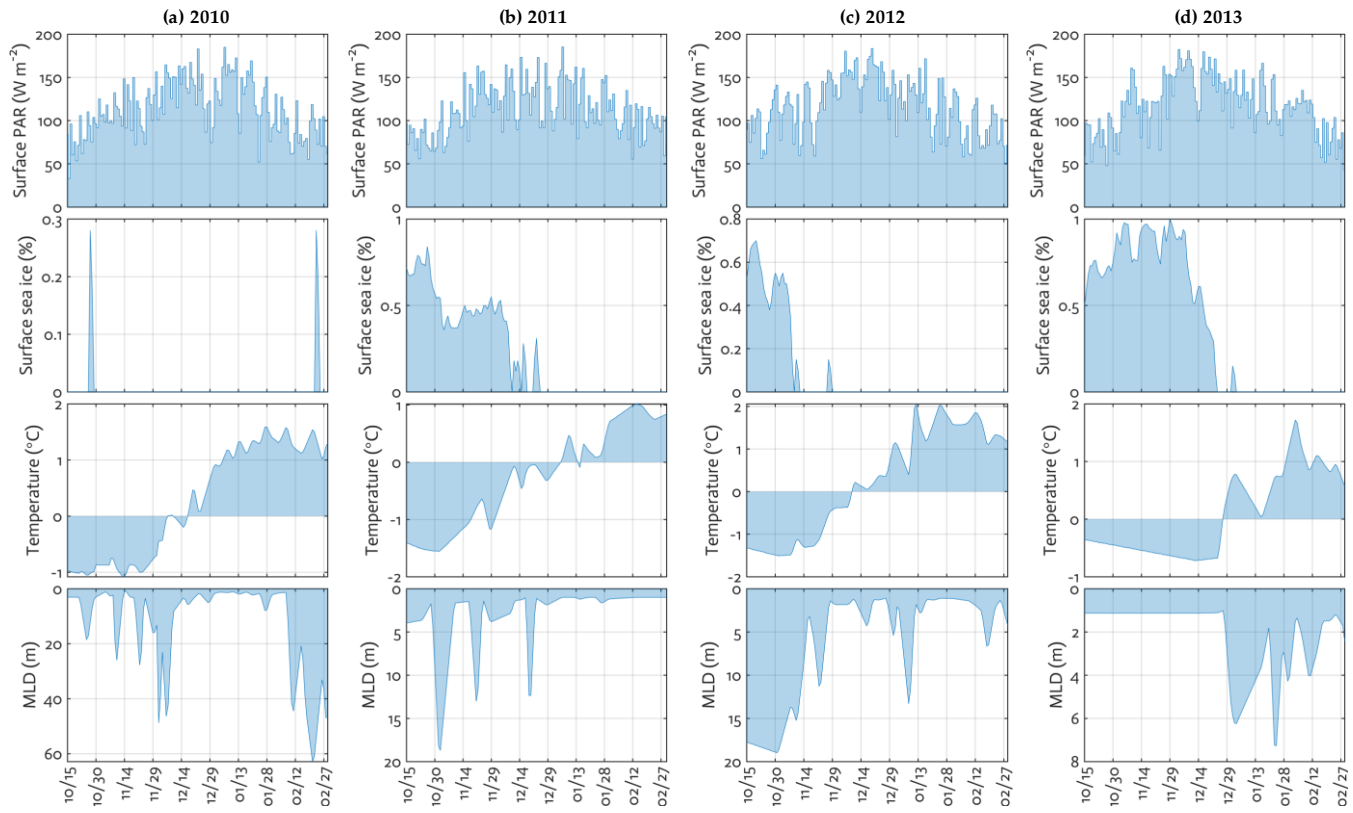


**Figure S2**

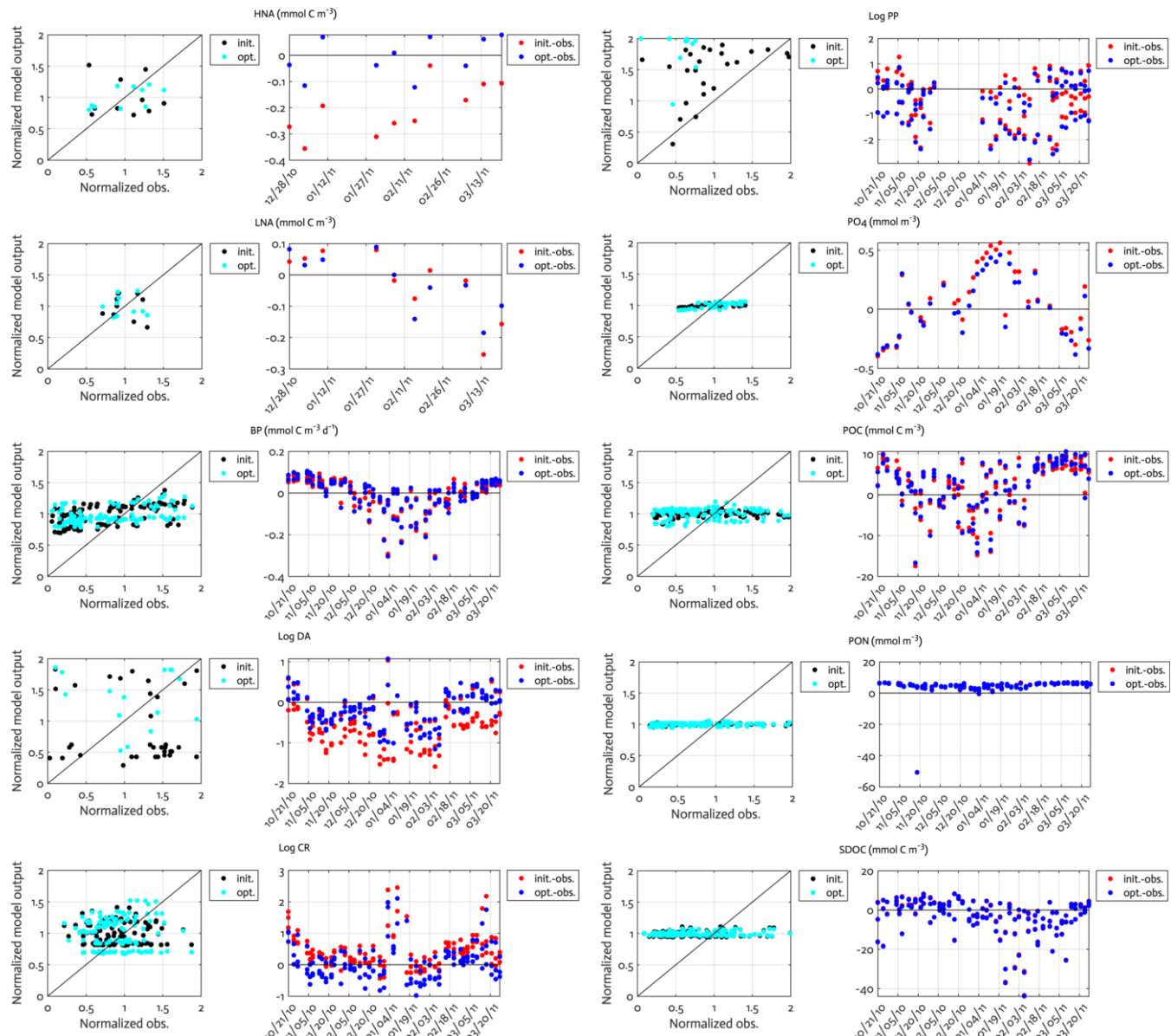


**Figure S3**

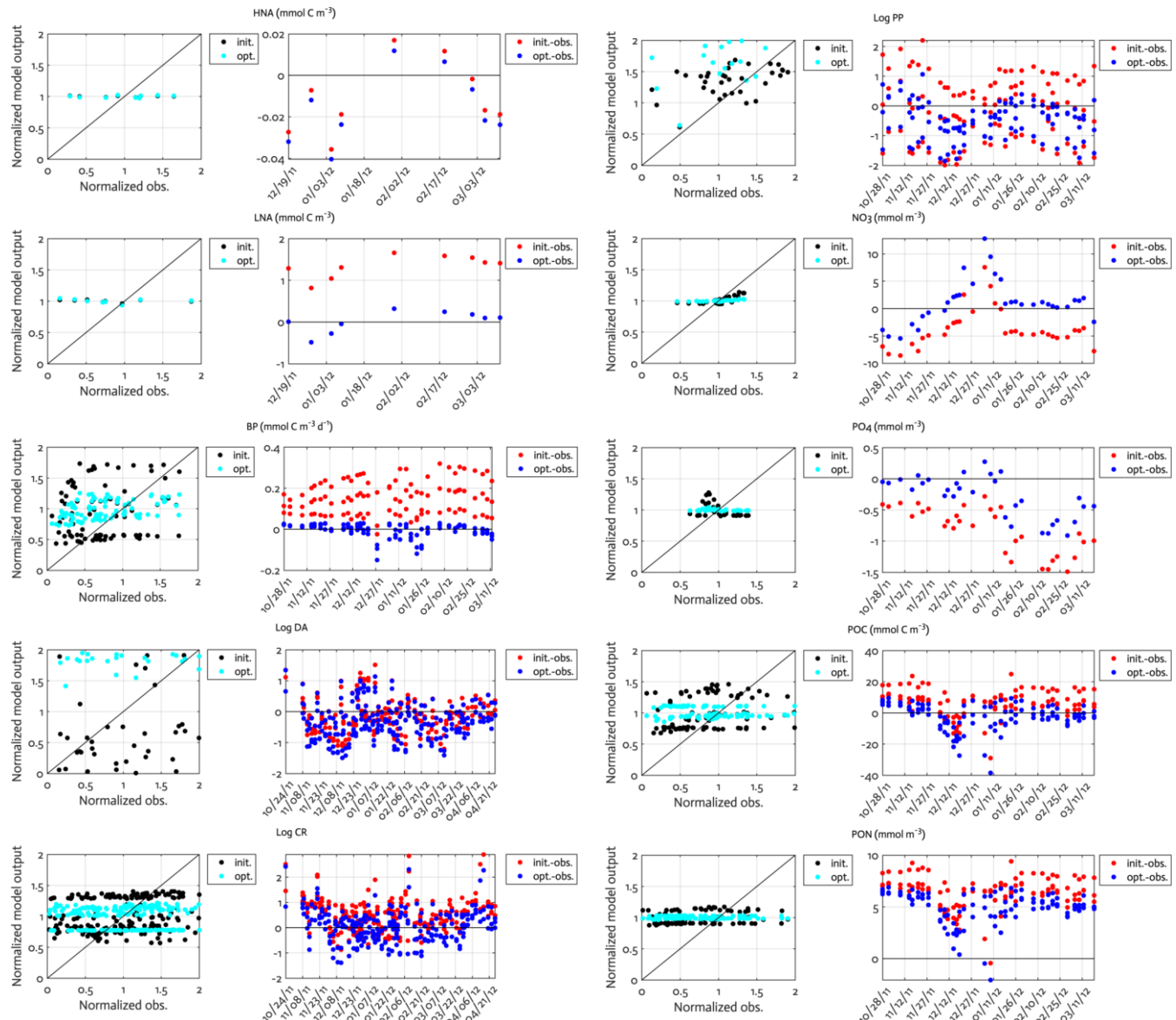


**Figure S4**

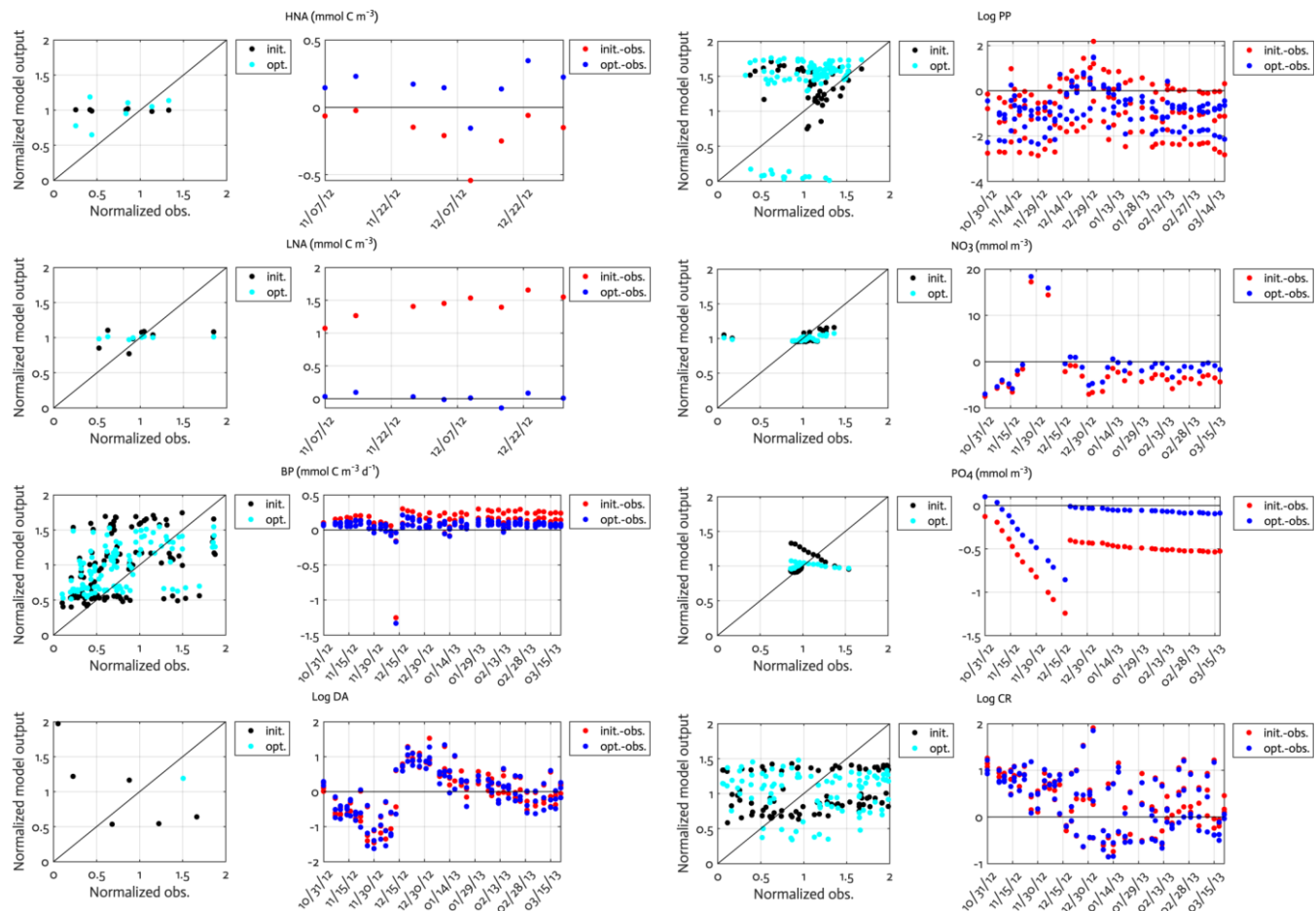


**Figure S5**

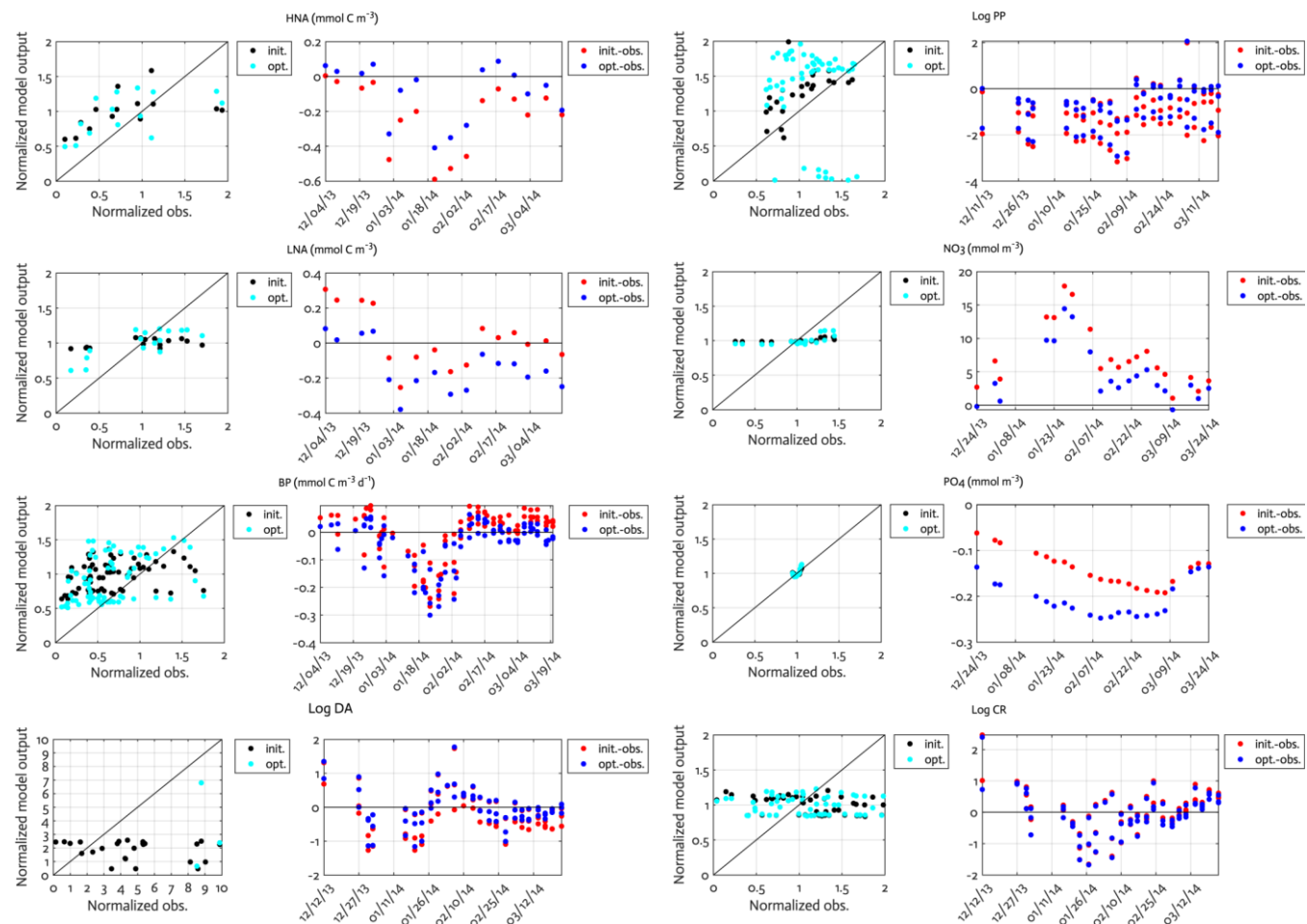


**Figure S6**

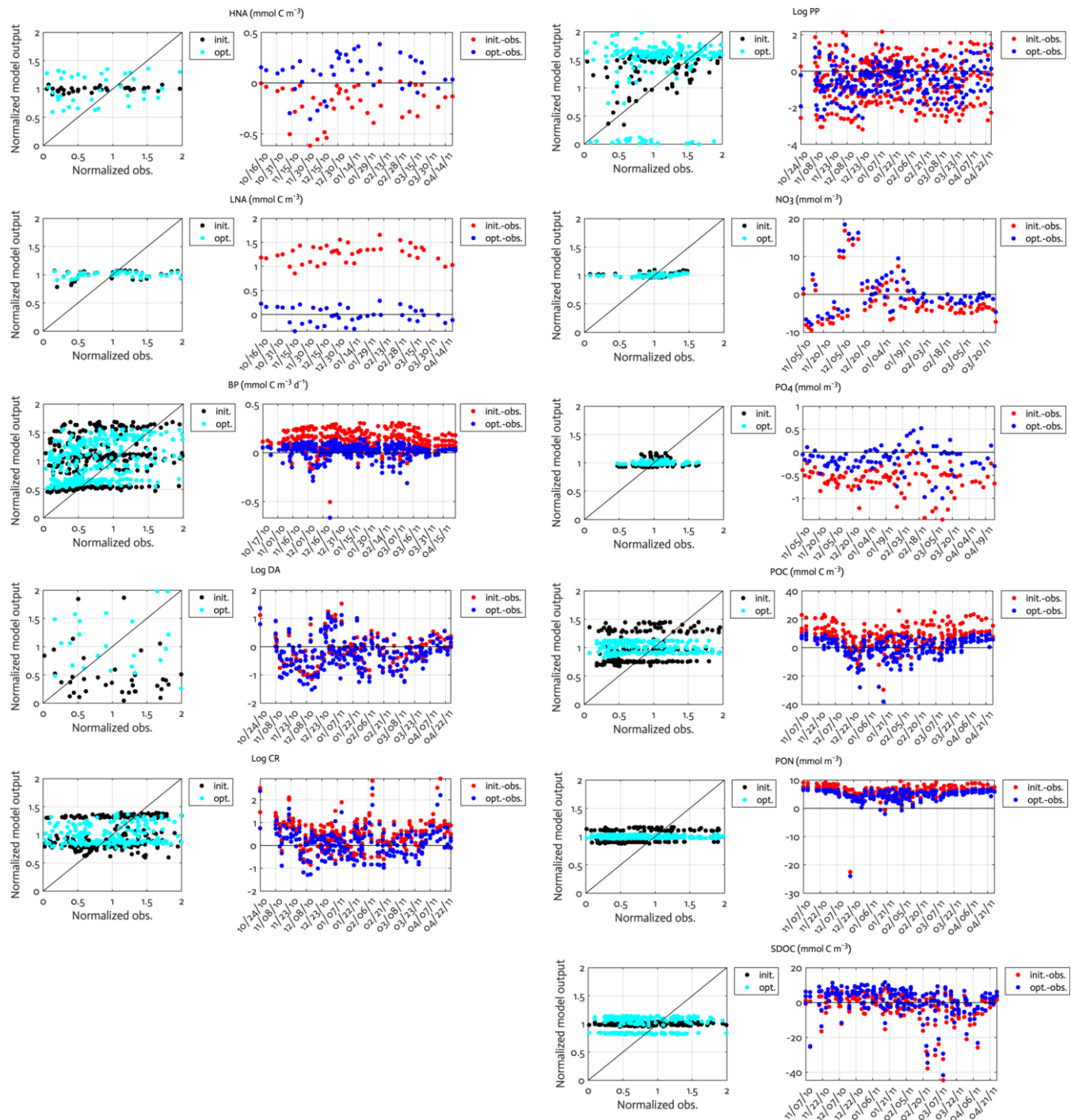


**Figure S7**

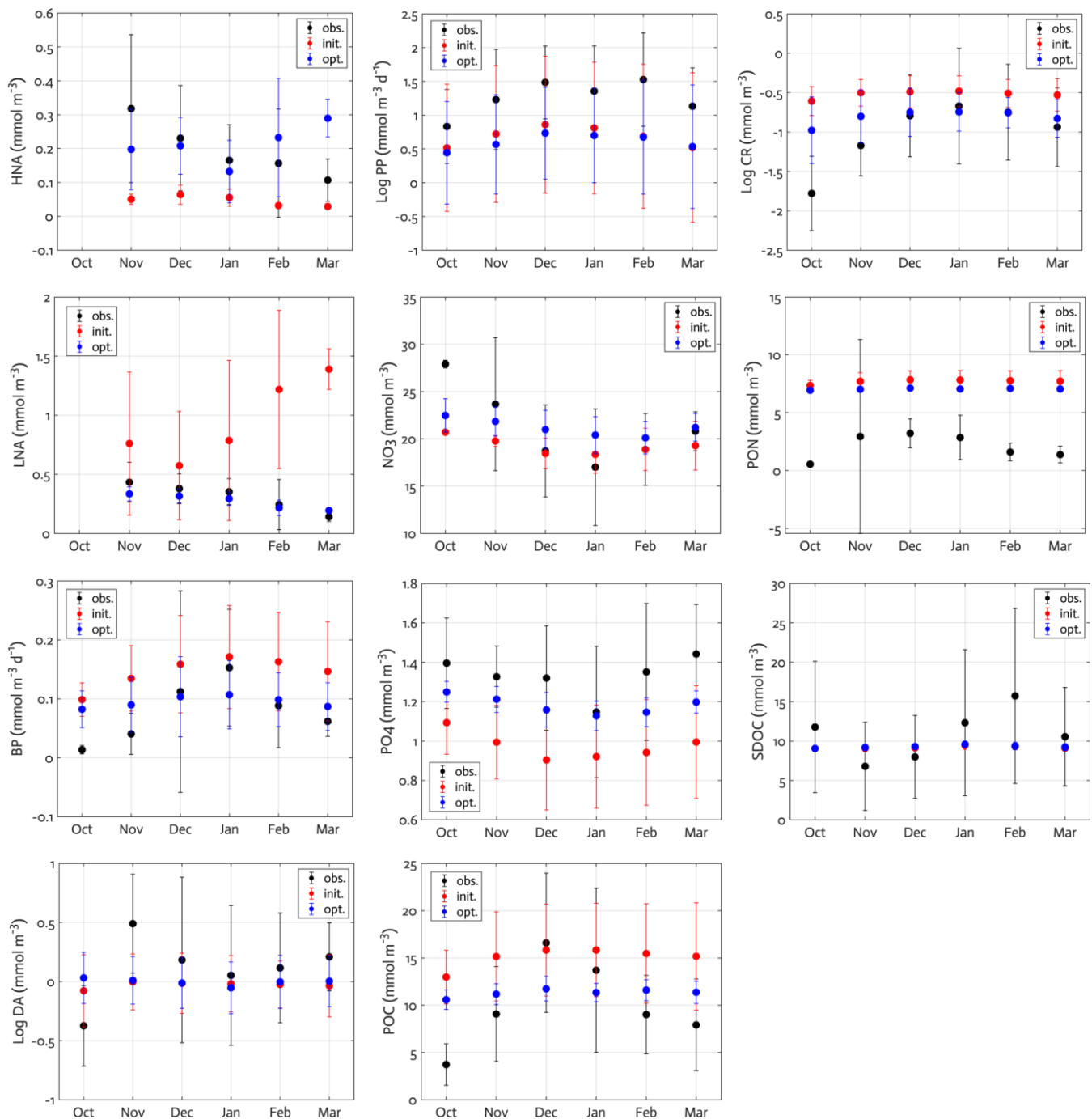


**Figure S8**

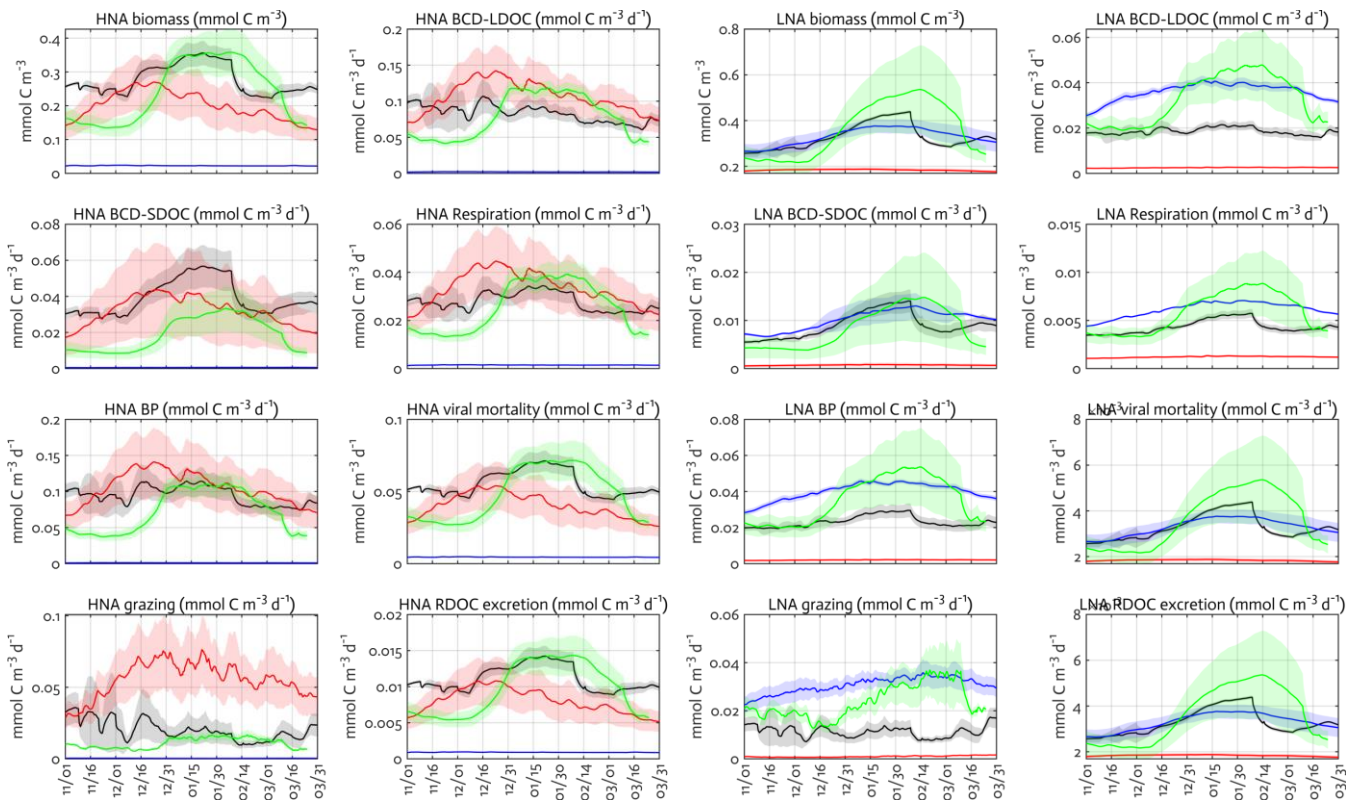


**Figure S9**

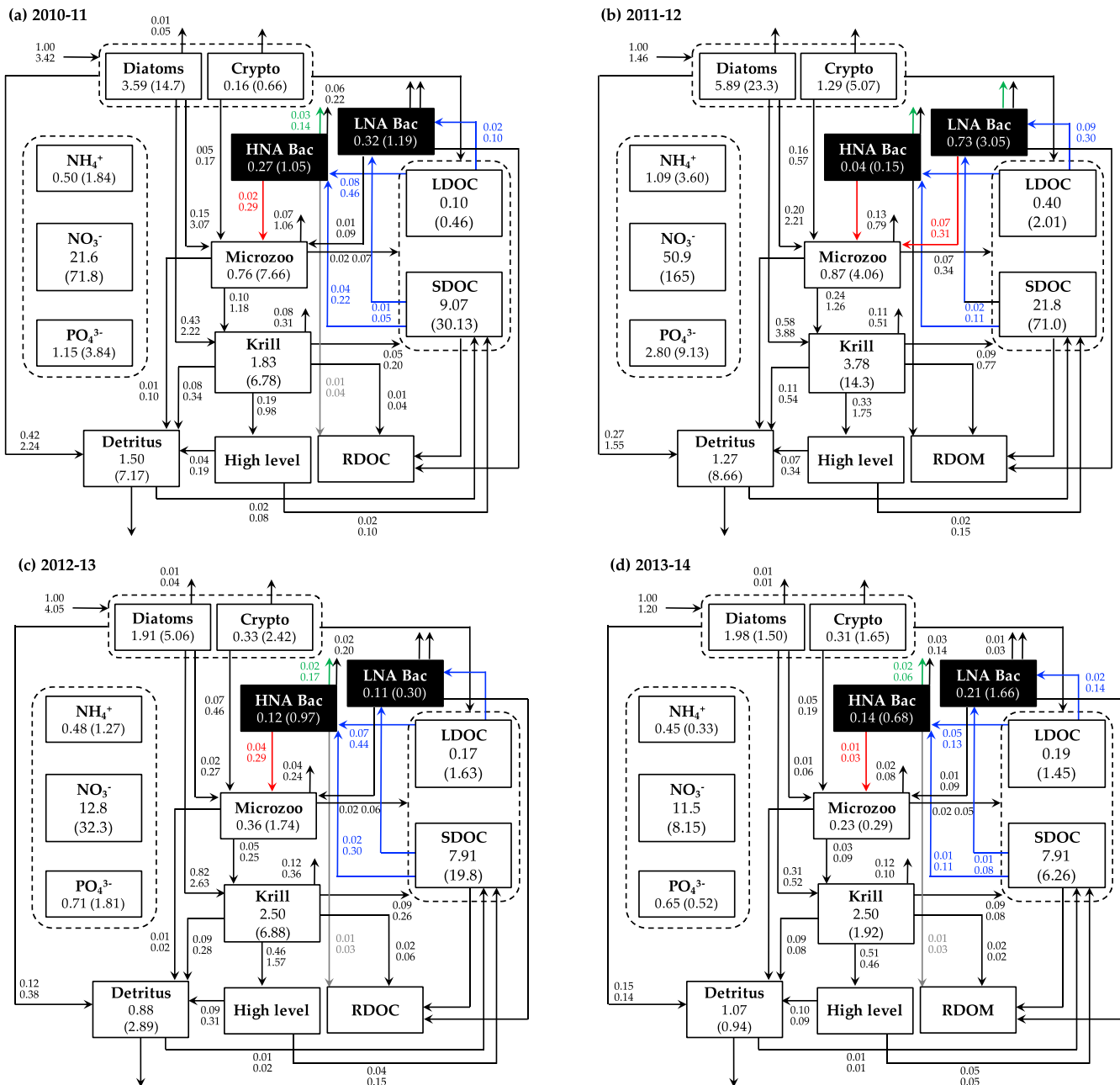


**Figure S10**

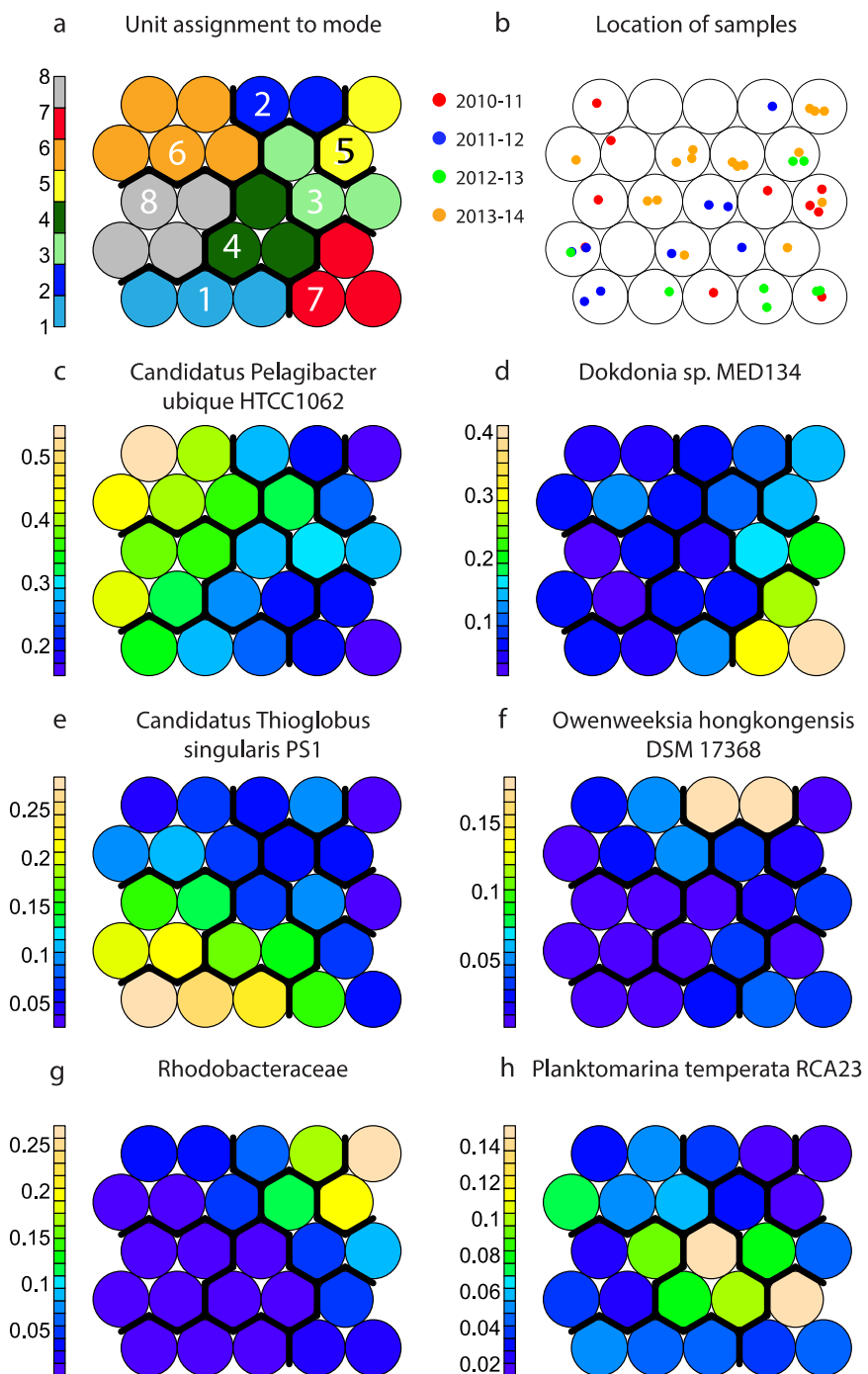


**Figure S11**

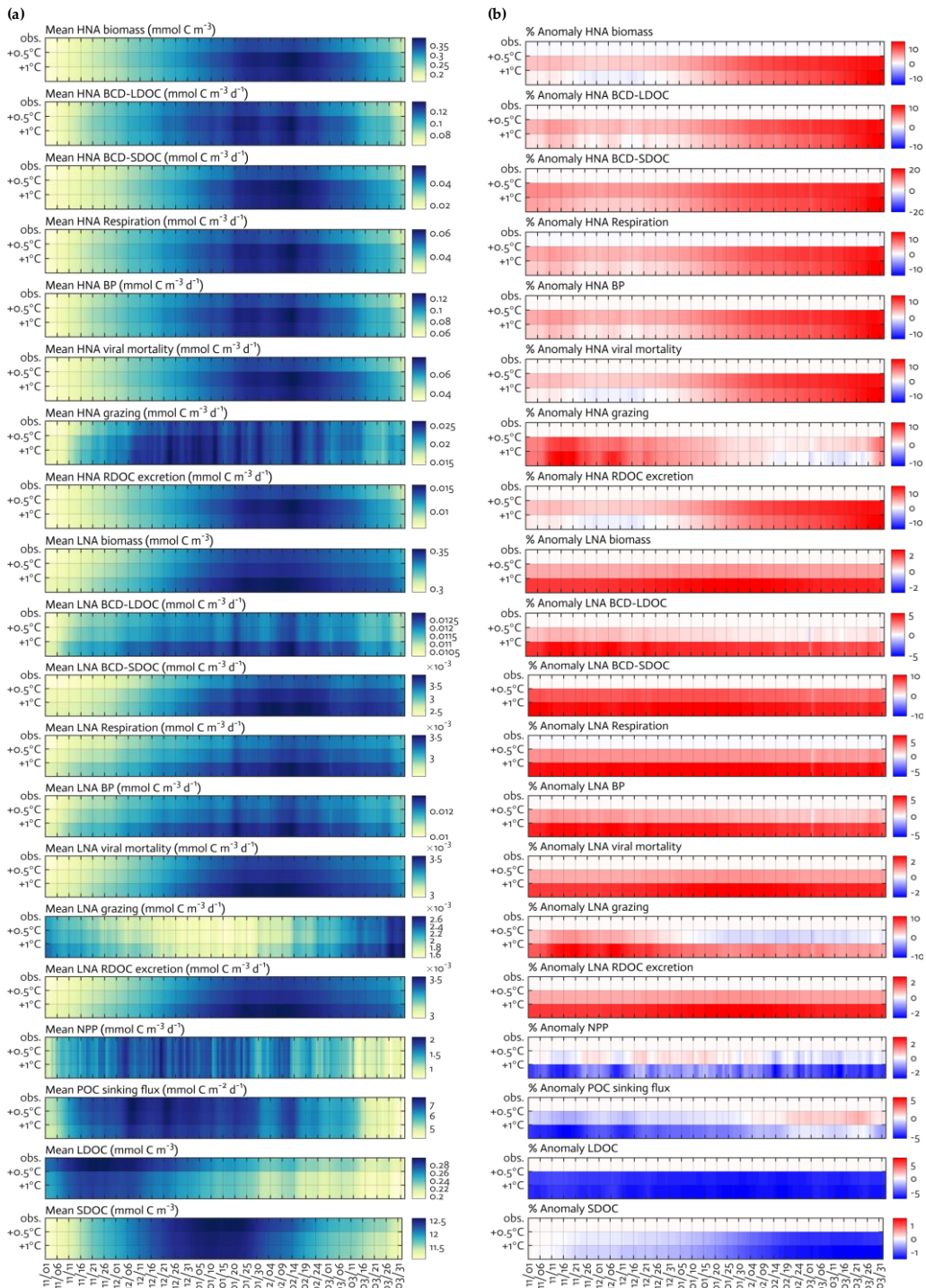


**Figure S12**

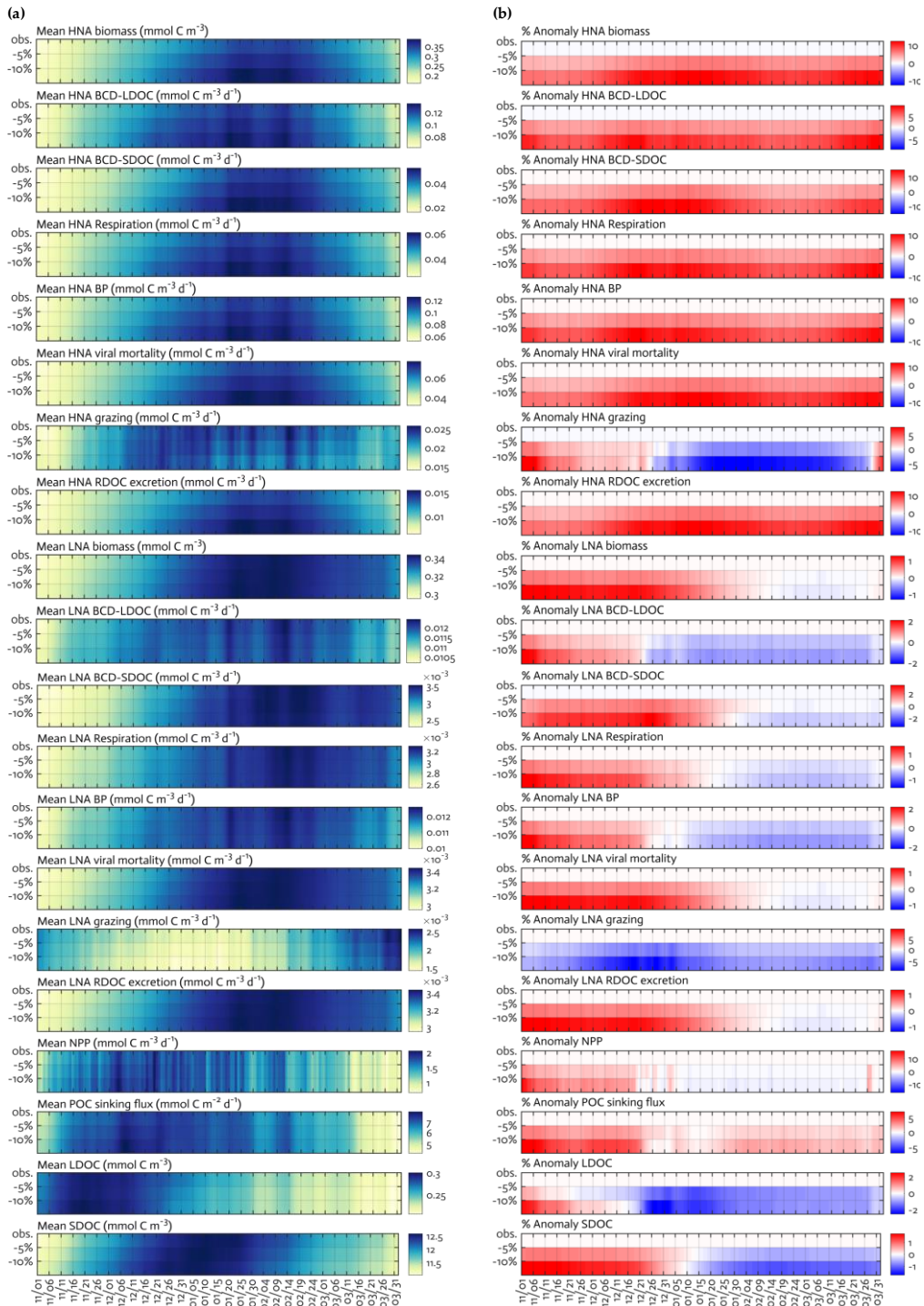


**Table S1**

Number of assimilated observations for each data type				
Data type	2010-11	2011-12	2012-13	2013-14
NO <sub>3</sub>	0	32	35	20
PO <sub>4</sub>	38	31	37	21
log <sub>10</sub> (Chl <sub>DA</sub> )	10	10	10	10
log <sub>10</sub> (Chl <sub>CR</sub> )	10	10	10	10
log <sub>10</sub> (PP)	35	34	40	23
HNA biomass	10	9	8	16
LNA biomass	10	9	8	16
BP	10	9	8	16
SDOC	45	34	0	0
POC	46	34	0	0
PON	46	34	0	0

**Table S2**

Model parameter	Init.	Opt.	Gradient	Mark
$A_E$ , Arrhenius parameter for temperature function	4000		1.02	
$\mu_{DA}$ , Diatom C-specific maximum growth rate, $d^{-1}$	2.0	0.86	-3.05E-02	CS
$\mu_{CR}$ , Crypto. C-specific maximum growth rate, $d^{-1}$	1.0		-0.589	
$\alpha_{DA}$ , Initial slope of P-I curve of diatoms, mol C ( $g\ Chl$ ) $^{-1}\ d^{-1}$ ( $W\ m^{-2}$ ) $^{-1}$	0.65	0.86	-1.80E-02	CS
$\alpha_{CR}$ , Initial slope of P-I curve of crypto., mol C ( $g\ Chl$ ) $^{-1}\ d^{-1}$ ( $W\ m^{-2}$ ) $^{-1}$	0.35		-0.268	
$\beta_{DA}$ , Light inhibition parameter for diatom photosynthesis ( $W\ m^{-2}$ ) $^{-1}$	0.005		-0.639	
$\beta_{CR}$ , Light inhibition parameter for crypto. photosynthesis ( $W\ m^{-2}$ ) $^{-1}$	0.005		-3.75E-03	
$v^N_{REF,DA}$ , Maximum N uptake rate per diatom C biomass, mol N ( $mol\ C$ ) $^{-1}\ d^{-1}$	0.5		0.38	
$v^N_{REF,CR}$ , Maximum N uptake rate per crypto. C biomass, mol N ( $mol\ C$ ) $^{-1}\ d^{-1}$	0.3		1.55E-02	
$k^{NH4}_{DA}$ , NH <sub>4</sub> half-saturation concentration for diatom uptake, mmol $m^{-3}$	0.1		0.744	
$k^{NH4}_{CR}$ , NH <sub>4</sub> half-saturation concentration for crypto. uptake, mmol $m^{-3}$	0.1		2.42E-02	
$k^{NO3}_{DA}$ , NO <sub>3</sub> half-saturation concentration for diatom uptake, mmol $m^{-3}$	0.9		-0.756	
$k^{NO3}_{CR}$ , NO <sub>3</sub> half-saturation concentration for crypto. uptake, mmol $m^{-3}$	0.6		-2.45E-02	
$v^P_{REF,DA}$ , Maximum P uptake rate per diatom C biomass, mol P ( $mol\ C$ ) $^{-1}\ d^{-1}$	0.03		-1.01	
$v^P_{REF,CR}$ , Maximum P uptake rate per crypto. C biomass, mol P ( $mol\ C$ ) $^{-1}\ d^{-1}$	0.03		-1.85E-02	
$k^{PO4}_{DA}$ , PO <sub>4</sub> half-saturation concentration for diatom uptake, mmol $m^{-3}$	0.05		4.58E-02	
$k^{PO4}_{CR}$ , PO <sub>4</sub> half-saturation concentration for crypto. uptake, mmol $m^{-3}$	0.04		6.74E-04	
$\zeta^{NO3}$ , C requirement (respiration) to assimilate NO <sub>3</sub> , mol C ( $mol\ N$ ) $^{-1}$	0.1		4.67	
$\Theta$ , Maximum Chl/N ratio, g Chl $a$ ( $mol\ N$ ) $^{-1}$	1.5	3.45	-5.34	OP
$expSV,DA$ , Diatom passive excretion rate per biomass, $d^{-1}$	0.00005		0.113	
$expSV,CR$ , Crypto. passive excretion rate per biomass, $d^{-1}$	0.00005		5.63E-03	
$exact,DA$ , Diatom active excretion rate per growth rate, $d^{-1}$	0.00005		-8.70E-04	
$exact,CR$ , Crypto. active excretion rate per growth rate, $d^{-1}$	0.00005		-8.80E-05	
$pom_{DA}$ , POM production rate by diatom aggregation, ( $mmol\ C\ m^{-3}$ ) $^{-1}d^{-1}$	0.03		-2.11	
$pom_{CR}$ , POM production rate by crypto. aggregation, ( $mmol\ C\ m^{-3}$ ) $^{-1}d^{-1}$	0.03		-4.54E-03	
$k^{DOC,HNA}$ , DOC half-saturation concentration for HNA bacterial uptake, mmol C $m^{-3}$	0.5		7.74E-03	
$k^{DOC,LNA}$ , DOC half-saturation concentration for LNA bacterial uptake, mmol C $m^{-3}$	0.2		0.324	
$rSDOC$ , Parameter controlling SDOC lability	0.005		-0.435	
$\mu_{HNA}$ , Maximum HNA bacterial growth rate, $d^{-1}$	2.0	3.97	0.416	CS
$\mu_{LNA}$ , Maximum LNA bacterial growth rate, $d^{-1}$	1.0	0.41	-1.55E-02	CS
$b_{R,HNA}$ , Parameter control HNA bacterial active respiration rate versus production, ( $mmol\ C\ m^{-3}\ d^{-1}$ ) $^{-1}$	0.08		-1.02E-02	
$b_{R,LNA}$ , Parameter control LNA bacterial active respiration rate versus production, ( $mmol\ C\ m^{-3}\ d^{-1}$ ) $^{-1}$	0.2		7.31E-04	
$exADJ,HNA$ , HNA bacterial extra SDOC excretion rate, $d^{-1}$	2.0		0	
$exADJ,LNA$ , LNA bacterial extra SDOC excretion rate, $d^{-1}$	2.0		0	
$remi_{HNA}$ , HNA bacterial nutrient regeneration rate, $d^{-1}$	8.0		0.279	
$remi_{LNA}$ , LNA bacterial nutrient regeneration rate, $d^{-1}$	2.0		0.343	
$exREFR,HNA$ , HNA bacterial RDOC production rate, $d^{-1}$	0.04		1.78E-02	
$exREFR,LNA$ , LNA bacterial RDOC production rate, $d^{-1}$	0.01		-0.106	
$f_S,HNA$ , HNA bacterial selection strength on SDOM	0.1		5.21E-03	
$f_S,LNA$ , LNA bacterial selection strength on SDOM	0.7		8.47E-03	
$r^B_{HNA}$ , HNA bacterial basal respiration rate, $d^{-1}$	0.04		0.103	
$r^B_{LNA}$ , LNA bacterial basal respiration rate, $d^{-1}$	0.01		4.48E-02	
$r^A_{min,HNA}$ , HNA bacterial minimum active respiration rate, $d^{-1}$	0.08		7.85E-03	
$r^A_{min,LNA}$ , LNA bacterial minimum active respiration rate, $d^{-1}$	0.04		-4.90E-04	
$r^A_{max,HNA}$ , HNA bacterial maximum active respiration rate, $d^{-1}$	0.4	0.18	-0.363	OP
$r^A_{max,LNA}$ , LNA bacterial maximum active respiration rate, $d^{-1}$	0.1		-2.85E-02	
$morth_{HNA}$ , HNA bacterial mortality rate, $d^{-1}$	0.2		-0.737	
$morth_{LNA}$ , LNA bacterial mortality rate, $d^{-1}$	0.01		-0.162	
$\mu_{MZ}$ , Microzoo. C-specific maximum growth rate, $d^{-1}$	2.5		-1.27	
$g_{DA}$ , Diatom half-saturation concentration in microzoo. grazing, mmol C $m^{-3}$	1.0		-1.33	
$g'_{DA}$ , Diatom half-saturation concentration in krill grazing, mmol C $m^{-3}$	1.0		-8.45E-02	

$g_{CR}$ , Crypto. half-saturation concentration in microzoo. grazing, mmol C m <sup>-3</sup>	1.0	0.12	2.00E-02	CS
$g_{HNA}$ , HNA bacterial half-saturation concentration in microzoo. grazing, mmol C m <sup>-3</sup>	0.55	0.37	2.23	OP
$g_{LNA}$ , LNA bacterial half-saturation concentration in microzoo. grazing, mmol C m <sup>-3</sup>	0.55		-0.688	
$ex_{MZ}$ , Total DOM excretion rate per microzoo. gross growth, d <sup>-1</sup>	0.15		3.51	
$f_{ex,MZ}$ , Fraction of LDOC of total microzoo. DOC excretion	0.75		4.37	
$r^B_{MZ}$ , Microzoo. basal respiration rate, d <sup>-1</sup>	0.01		-7.21E-02	
$r^A_{MZ}$ , Microzoo. active respiration rate, d <sup>-1</sup>	0.30		-1.83	
$exADJ_{MZ}$ , Microzoo. extra SDOM excretion rate, d <sup>-1</sup>	2.0		0	
$remi_{MZ}$ , Microzoo. nutrient regeneration rate, d <sup>-1</sup>	4.68		-8.09E-02	
$pom_{MZ}$ , POM production rate per microzoo. gross growth, d <sup>-1</sup>	0.03		-9.01E-02	
$\mu_{KR}$ , Maximum krill C-specific growth rate, d <sup>-1</sup>	0.7	0.97	-1.46	OP
$g_{MZ}$ , Microzoo. half-saturation concentration in krill grazing, mmol C m <sup>-3</sup>	0.5	0.41	0.529	CS
$ex_{KR}$ , Total DOM excretion rate per krill gross growth, d <sup>-1</sup>	0.1		-1.76	
$f_{ex,KR}$ , Fraction of labile DOC of total krill DOC excretion	0.25		-0.2	
$r^B_{KR}$ , Krill basal respiration rate, d <sup>-1</sup>	0.03		0.366	
$r^A_{KR}$ , Krill active respiration rate, d <sup>-1</sup>	0.09		0.69	
$exADJ_{KR}$ , Krill extra SDOM excretion rate, d <sup>-1</sup>	2.0		0	
$remi_{KR}$ , Krill nutrient regeneration rate, d <sup>-1</sup>	4.0		9.49E-02	
$pom_{KR}$ , POM production rate per krill gross growth, d <sup>-1</sup>	0.15		1.71	
$exREFR_{KR}$ , Krill RDOC production rate, d <sup>-1</sup>	0.02		0.148	
$remv_{KR}$ , Krill removal rate by higher-trophic levels, (mmol C m <sup>-3</sup> ) <sup>-1</sup> d <sup>-1</sup>	0.05		-3.83	
$f_{KR}$ , Fraction of SDOM production by krill	0.1		-0.96	
$f_{POM,HZ}$ , Fraction of POM production by higher-trophic level	0.2		3.16E-02	
$exREFRSDOM$ , Conversion rate of SDOM to RDOM, d <sup>-1</sup>	0.0009		4.17E-02	
$q^C_{N,RDOM}$ , RDOM N/C ratio, mol N (mol C) <sup>-1</sup>	0.05		0.1	
$q^C_{P,RDOM}$ , RDOM P/C ratio, mol P (mol C) <sup>-1</sup>	0.00065		-1.18E-02	
$q^C_{N,POM}$ , N/C ratio for POM production by microzoo. and krill, mol N (mol C) <sup>-1</sup>	0.12		0.508	
$q^C_{P,POM}$ , P/C ratio for POM production by microzoo. and krill, mol P (mol C) <sup>-1</sup>	0.00045		-0.323	
$r_{nitr}$ , Nitrification rate (NH <sub>4</sub> to NO <sub>3</sub> ), d <sup>-1</sup>	0.076		0.187	
$prf_N$ , Preference for dissolving N content in POM	1.1		-0.145	
$prf_P$ , Preference for dissolving P content in POM	4.0		6.39E-02	
$wnsv$ , Detritus vertical sinking velocity, m d <sup>-1</sup>	6.0		-7.14	
$diss$ , Detrital dissolution rate, d <sup>-1</sup>	0.01		-0.607	

**Table S3**

Model parameter	Init.	Opt.	Gradient	Mark
$A_E$ , Arrhenius parameter for temperature function	4000		1.33	
$\mu_{DA}$ , Diatom C-specific maximum growth rate, $d^{-1}$	2.0	0.61	-2.36E-07	CS
$\mu_{CR}$ , Crypto. C-specific maximum growth rate, $d^{-1}$	1.0		0.206	
$a_{DA}$ , Initial slope of P-I curve of diatoms, mol C (g Chl) $^{-1}$ $d^{-1}$ ( $W\ m^{-2}$ ) $^{-1}$	0.65	0.45	2.96E-02	OP
$a_{CR}$ , Initial slope of P-I curve of crypto., mol C (g Chl) $^{-1}$ $d^{-1}$ ( $W\ m^{-2}$ ) $^{-1}$	0.35		5.22E-02	
$\beta_{DA}$ , Light inhibition parameter for diatom photosynthesis ( $W\ m^{-2}$ ) $^{-1}$	0.005		-6.88E-02	
$\beta_{CR}$ , Light inhibition parameter for crypto. photosynthesis ( $W\ m^{-2}$ ) $^{-1}$	0.005		3.57E-02	
$v^N_{REF,DA}$ , Maximum N uptake rate per diatom C biomass, mol N (mol C) $^{-1}$ $d^{-1}$	0.5		6.26E-02	
$v^N_{REF,CR}$ , Maximum N uptake rate per crypto. C biomass, mol N (mol C) $^{-1}$ $d^{-1}$	0.3		2.30E-02	
$k^{NH4}_{DA}$ , NH <sub>4</sub> half-saturation concentration for diatom uptake, mmol m $^{-3}$	0.1		-0.122	
$k^{NH4}_{CR}$ , NH <sub>4</sub> half-saturation concentration for crypto. uptake, mmol m $^{-3}$	0.1		-4.15E-02	
$k^{NO3}_{DA}$ , NO <sub>3</sub> half-saturation concentration for diatom uptake, mmol m $^{-3}$	0.9		0.12	
$k^{NO3}_{CR}$ , NO <sub>3</sub> half-saturation concentration for crypto. uptake, mmol m $^{-3}$	0.6		4.10E-02	
$v^P_{REF,DA}$ , Maximum P uptake rate per diatom C biomass, mol P (mol C) $^{-1}$ $d^{-1}$	0.03	0.02	1.58	OP
$v^P_{REF,CR}$ , Maximum P uptake rate per crypto. C biomass, mol P (mol C) $^{-1}$ $d^{-1}$	0.03		0.244	
$k^{PO4}_{DA}$ , PO <sub>4</sub> half-saturation concentration for diatom uptake, mmol m $^{-3}$	0.05		-6.01E-02	
$k^{PO4}_{CR}$ , PO <sub>4</sub> half-saturation concentration for crypto. uptake, mmol m $^{-3}$	0.04		-7.54E-03	
$\zeta^{NO3}$ , C requirement (respiration) to assimilate NO <sub>3</sub> , mol C (mol N) $^{-1}$	0.1		0.683	
$\Theta$ , Maximum Chl/N ratio, g Chl <i>a</i> (mol N) $^{-1}$	1.5		-7.86	
$expSV,DA$ , Diatom passive excretion rate per biomass, $d^{-1}$	0.00005		3.64E-02	
$expSV,CR$ , Crypto. passive excretion rate per biomass, $d^{-1}$	0.00005		5.40E-03	
$exact,DA$ , Diatom active excretion rate per growth rate, $d^{-1}$	0.00005		-5.24E-04	
$exact,CR$ , Crypto. active excretion rate per growth rate, $d^{-1}$	0.00005		1.29E-04	
$pom_{DA}$ , POM production rate by diatom aggregation, (mmol C m $^{-3}$ ) $^{-1}$ $d^{-1}$	0.03		7.33	
$pom_{CR}$ , POM production rate by crypto. aggregation, (mmol C m $^{-3}$ ) $^{-1}$ $d^{-1}$	0.03		0.44	
$k^{DOC,HNA}$ , DOC half-saturation concentration for HNA bacterial uptake, mmol C m $^{-3}$	0.5		2.78E-02	
$k^{DOC,LNA}$ , DOC half-saturation concentration for LNA bacterial uptake, mmol C m $^{-3}$	0.2		-1.63	
$r_{SDOC}$ , Parameter controlling SDOC lability	0.005		1.03	
$\mu_{HNA}$ , Maximum HNA bacterial growth rate, $d^{-1}$	2.0	0.76	-6.53E-03	OP
$\mu_{LNA}$ , Maximum LNA bacterial growth rate, $d^{-1}$	1.0	0.56	4.45E-07	CS
$b_{RHNA}$ , Parameter control HNA bacterial active respiration rate versus production, (mmol C m $^{-3}$ $d^{-1}$ ) $^{-1}$	0.08		-2.76E-05	
$b_{RLNA}$ , Parameter control LNA bacterial active respiration rate versus production, (mmol C m $^{-3}$ $d^{-1}$ ) $^{-1}$	0.2		1.27E-03	
$exADJ,HNA$ , HNA bacterial extra SDOC excretion rate, $d^{-1}$	2.0		0	
$exADJ,LNA$ , LNA bacterial extra SDOC excretion rate, $d^{-1}$	2.0		0	
$remiHNA$ , HNA bacterial nutrient regeneration rate, $d^{-1}$	8.0		-0.189	
$remiLNA$ , LNA bacterial nutrient regeneration rate, $d^{-1}$	2.0	2.22	-3.26	OP
$exREFR,HNA$ , HNA bacterial RDOC production rate, $d^{-1}$	0.04		8.34E-02	
$exREFR,LNA$ , LNA bacterial RDOC production rate, $d^{-1}$	0.01		-0.141	
$f_{S,HNA}$ , HNA bacterial selection strength on SDOM	0.1		-1.49E-03	
$f_{S,LNA}$ , LNA bacterial selection strength on SDOM	0.7		-8.81E-02	
$r^B_{HNA}$ , HNA bacterial basal respiration rate, $d^{-1}$	0.04		3.70E-02	
$r^B_{LNA}$ , LNA bacterial basal respiration rate, $d^{-1}$	0.01		-0.143	
$r^A_{min,HNA}$ , HNA bacterial minimum active respiration rate, $d^{-1}$	0.08		6.89E-06	
$r^A_{min,LNA}$ , LNA bacterial minimum active respiration rate, $d^{-1}$	0.04		-8.56E-04	
$r^A_{max,HNA}$ , HNA bacterial maximum active respiration rate, $d^{-1}$	0.4		0.116	
$r^A_{max,LNA}$ , LNA bacterial maximum active respiration rate, $d^{-1}$	0.1		-1.30E-02	
$morth_{HNA}$ , HNA bacterial mortality rate, $d^{-1}$	0.2		0.63	
$morth_{LNA}$ , LNA bacterial mortality rate, $d^{-1}$	0.01		0.334	
$\mu_{MZ}$ , Microzoo. C-specific maximum growth rate, $d^{-1}$	2.5		1.16	
$g_{DA}$ , Diatom half-saturation concentration in microzoo. grazing, mmol C m $^{-3}$	1.0	2.33	2.32E-07	CS
$g'_{DA}$ , Diatom half-saturation concentration in krill grazing, mmol C m $^{-3}$	1.0		-3.43	

$g_{CR}$ , Crypto. half-saturation concentration in microzoo. grazing, mmol C m <sup>-3</sup>	1.0	0.61	-3.73E-07	CS
$g_{HNA}$ , HNA bacterial half-saturation concentration in microzoo. grazing, mmol C m <sup>-3</sup>	0.55	0.37	-0.157	OP
$g_{LNA}$ , LNA bacterial half-saturation concentration in microzoo. grazing, mmol C m <sup>-3</sup>	0.55		0.721	
$ex_{MZ}$ , Total DOM excretion rate per microzoo. gross growth, d <sup>-1</sup>	0.15		0.27	
$f_{ex,MZ}$ , Fraction of LDOC of total microzoo. DOC excretion	0.75		-3.7	
$r^B_{MZ}$ , Microzoo. basal respiration rate, d <sup>-1</sup>	0.01		-2.81E-02	
$r^A_{MZ}$ , Microzoo. active respiration rate, d <sup>-1</sup>	0.30		-1.8	
$exADJ_{MZ}$ , Microzoo. extra SDOM excretion rate, d <sup>-1</sup>	2.0		0	
$remi_{MZ}$ , Microzoo. nutrient regeneration rate, d <sup>-1</sup>	4.68		-0.306	
$pom_{MZ}$ , POM production rate per microzoo. gross growth, d <sup>-1</sup>	0.03		-9.11E-02	
$\mu_{KR}$ , Maximum krill C-specific growth rate, d <sup>-1</sup>	0.7	0.94	-2.81	OP
$g_{MZ}$ , Microzoo. half-saturation concentration in krill grazing, mmol C m <sup>-3</sup>	0.5	0.23	-3.31E-07	CS
$ex_{KR}$ , Total DOM excretion rate per krill gross growth, d <sup>-1</sup>	0.1		3.24	
$f_{ex,KR}$ , Fraction of labile DOC of total krill DOC excretion	0.25		-0.483	
$r^B_{KR}$ , Krill basal respiration rate, d <sup>-1</sup>	0.03		-0.354	
$r^A_{KR}$ , Krill active respiration rate, d <sup>-1</sup>	0.09		-2.04E-02	
$exADJ_{KR}$ , Krill extra SDOM excretion rate, d <sup>-1</sup>	2.0		0	
$remi_{KR}$ , Krill nutrient regeneration rate, d <sup>-1</sup>	4.0		-0.498	
$pom_{KR}$ , POM production rate per krill gross growth, d <sup>-1</sup>	0.15		0.72	
$exREFR_{KR}$ , Krill RDOC production rate, d <sup>-1</sup>	0.02		1.66E-03	
$remv_{KR}$ , Krill removal rate by higher-trophic levels, (mmol C m <sup>-3</sup> ) <sup>-1</sup> d <sup>-1</sup>	0.05		-0.494	
$f_{KR}$ , Fraction of SDOM production by krill	0.1		0.707	
$f_{POM,HZ}$ , Fraction of POM production by higher-trophic level	0.2		1.07	
$exREFRSDOM$ , Conversion rate of SDOM to RDOM, d <sup>-1</sup>	0.0009		-2.71E-02	
$q^C_{N,RDOM}$ , RDOM N/C ratio, mol N (mol C) <sup>-1</sup>	0.05		-8.86E-02	
$q^C_{P,RDOM}$ , RDOM P/C ratio, mol P (mol C) <sup>-1</sup>	0.00065		4.01E-02	
$q^C_{N,POM}$ , N/C ratio for POM production by microzoo. and krill, mol N (mol C) <sup>-1</sup>	0.12		1.39E-02	
$q^C_{P,POM}$ , P/C ratio for POM production by microzoo. and krill, mol P (mol C) <sup>-1</sup>	0.00045		1.46	
$r_{nitr}$ , Nitrification rate (NH <sub>4</sub> to NO <sub>3</sub> ), d <sup>-1</sup>	0.076		0.785	
$prf_N$ , Preference for dissolving N content in POM	1.1		-4.44E-02	
$prf_P$ , Preference for dissolving P content in POM	4.0		-2.04E-02	
$wnsv$ , Detritus vertical sinking velocity, m d <sup>-1</sup>	6.0		0.426	
$diss$ , Detrital dissolution rate, d <sup>-1</sup>	0.01		2.96E-02	

**Table S4**

Model parameter	Init.	Opt.	Gradient	Mark
$A_E$ , Arrhenius parameter for temperature function	4000		1.17	
$\mu_{DA}$ , Diatom C-specific maximum growth rate, $d^{-1}$	2.0	1.34	5.71	OP
$\mu_{CR}$ , Crypto. C-specific maximum growth rate, $d^{-1}$	1.0		-1.97	
$a_{DA}$ , Initial slope of P-I curve of diatoms, mol C (g Chl) $^{-1}$ $d^{-1}$ ( $W m^{-2}$ ) $^{-1}$	0.65	1.78	0.101	CS
$a_{CR}$ , Initial slope of P-I curve of crypto., mol C (g Chl) $^{-1}$ $d^{-1}$ ( $W m^{-2}$ ) $^{-1}$	0.35		-1.3	
$\beta_{DA}$ , Light inhibition parameter for diatom photosynthesis ( $W m^{-2}$ ) $^{-1}$	0.005		0.531	
$\beta_{CR}$ , Light inhibition parameter for crypto. photosynthesis ( $W m^{-2}$ ) $^{-1}$	0.005		0.625	
$v^N_{REF,DA}$ , Maximum N uptake rate per diatom C biomass, mol N (mol C) $^{-1}$ $d^{-1}$	0.5		4.70E-02	
$v^N_{REF,CR}$ , Maximum N uptake rate per crypto. C biomass, mol N (mol C) $^{-1}$ $d^{-1}$	0.3		1.93E-02	
$k^{NH4}_{DA}$ , NH <sub>4</sub> half-saturation concentration for diatom uptake, mmol m $^{-3}$	0.1		0.147	
$k^{NH4}_{CR}$ , NH <sub>4</sub> half-saturation concentration for crypto. uptake, mmol m $^{-3}$	0.1		6.14E-03	
$k^{NO3}_{DA}$ , NO <sub>3</sub> half-saturation concentration for diatom uptake, mmol m $^{-3}$	0.9		-0.149	
$k^{NO3}_{CR}$ , NO <sub>3</sub> half-saturation concentration for crypto. uptake, mmol m $^{-3}$	0.6		-6.51E-03	
$v^P_{REF,DA}$ , Maximum P uptake rate per diatom C biomass, mol P (mol C) $^{-1}$ $d^{-1}$	0.03		2.73	
$v^P_{REF,CR}$ , Maximum P uptake rate per crypto. C biomass, mol P (mol C) $^{-1}$ $d^{-1}$	0.03		0.168	
$k^{PO4}_{DA}$ , PO <sub>4</sub> half-saturation concentration for diatom uptake, mmol m $^{-3}$	0.05		-0.112	
$k^{PO4}_{CR}$ , PO <sub>4</sub> half-saturation concentration for crypto. uptake, mmol m $^{-3}$	0.04		-5.64E-03	
$\zeta^{NO3}$ , C requirement (respiration) to assimilate NO <sub>3</sub> , mol C (mol N) $^{-1}$	0.1		0.32	
$\Theta$ , Maximum Chl/N ratio, g Chl <i>a</i> (mol N) $^{-1}$	1.5	4.39	5.86E-03	CS
$expSV,DA$ , Diatom passive excretion rate per biomass, $d^{-1}$	0.00005		2.48E-02	
$expSV,CR$ , Crypto. passive excretion rate per biomass, $d^{-1}$	0.00005		7.75E-04	
$exact,DA$ , Diatom active excretion rate per growth rate, $d^{-1}$	0.00005		2.18E-04	
$exact,CR$ , Crypto. active excretion rate per growth rate, $d^{-1}$	0.00005		-3.05E-04	
$pom_{DA}$ , POM production rate by diatom aggregation, (mmol C m $^{-3}$ ) $^{-1}$ $d^{-1}$	0.03		2.4	
$pom_{CR}$ , POM production rate by crypto. aggregation, (mmol C m $^{-3}$ ) $^{-1}$ $d^{-1}$	0.03		0.225	
$k^{DOC,HNA}$ , DOC half-saturation concentration for HNA bacterial uptake, mmol C m $^{-3}$	0.5		-0.111	
$k^{DOC,LNA}$ , DOC half-saturation concentration for LNA bacterial uptake, mmol C m $^{-3}$	0.2		2.43E-02	
$r_{SDOC}$ , Parameter controlling SDOC lability	0.005		-0.863	
$\mu_{HNA}$ , Maximum HNA bacterial growth rate, $d^{-1}$	2.0	3.67	-0.206	CS
$\mu_{LNA}$ , Maximum LNA bacterial growth rate, $d^{-1}$	1.0	0.06	-3.32E-02	CS
$b_{RHNA}$ , Parameter control HNA bacterial active respiration rate versus production, (mmol C m $^{-3}$ $d^{-1}$ ) $^{-1}$	0.08		-2.37E-02	
$b_{RLNA}$ , Parameter control LNA bacterial active respiration rate versus production, (mmol C m $^{-3}$ $d^{-1}$ ) $^{-1}$	0.2		-6.19E-06	
$exAD,HNA$ , HNA bacterial extra SDOC excretion rate, $d^{-1}$	2.0		0	
$exAD,LNA$ , LNA bacterial extra SDOC excretion rate, $d^{-1}$	2.0		0	
$remiHNA$ , HNA bacterial nutrient regeneration rate, $d^{-1}$	8.0		-1.05	
$remiLNA$ , LNA bacterial nutrient regeneration rate, $d^{-1}$	2.0		-0.164	
$exREFR,HNA$ , HNA bacterial RDOC production rate, $d^{-1}$	0.04		-0.195	
$exREFR,LNA$ , LNA bacterial RDOC production rate, $d^{-1}$	0.01		-3.84E-03	
$f_S,HNA$ , HNA bacterial selection strength on SDOM	0.1		-1.10E-02	
$f_S,LNA$ , LNA bacterial selection strength on SDOM	0.7		-4.22E-03	
$r^B_{HNA}$ , HNA bacterial basal respiration rate, $d^{-1}$	0.04		7.18E-02	
$r^B_{LNA}$ , LNA bacterial basal respiration rate, $d^{-1}$	0.01		2.76E-02	
$r^A_{min,HNA}$ , HNA bacterial minimum active respiration rate, $d^{-1}$	0.08		1.42E-02	
$r^A_{min,LNA}$ , LNA bacterial minimum active respiration rate, $d^{-1}$	0.04		4.13E-06	
$r^A_{max,HNA}$ , HNA bacterial maximum active respiration rate, $d^{-1}$	0.4	0.21	0.783	OP
$r^A_{max,LNA}$ , LNA bacterial maximum active respiration rate, $d^{-1}$	0.1		8.52E-03	
$morth_{HNA}$ , HNA bacterial mortality rate, $d^{-1}$	0.2		-1.32	
$morth_{LNA}$ , LNA bacterial mortality rate, $d^{-1}$	0.01		7.22E-02	
$\mu_{MZ}$ , Microzoo. C-specific maximum growth rate, $d^{-1}$	2.5		2.93	
$g_{DA}$ , Diatom half-saturation concentration in microzoo. grazing, mmol C m $^{-3}$	1.0		-4.69E-02	
$g_{DA}$ , Diatom half-saturation concentration in krill grazing, mmol C m $^{-3}$	1.0		10.4	

$g_{CR}$ , Crypto. half-saturation concentration in microzoo. grazing, mmol C m <sup>-3</sup>	1.0	0.14	-0.252	CS
$g_{HNA}$ , HNA bacterial half-saturation concentration in microzoo. grazing, mmol C m <sup>-3</sup>	0.55	0.08	-2.12E-02	CS
$g_{LNA}$ , LNA bacterial half-saturation concentration in microzoo. grazing, mmol C m <sup>-3</sup>	0.55		0.337	
$ex_{MZ}$ , Total DOM excretion rate per microzoo. gross growth, d <sup>-1</sup>	0.15		-3.14	
$f_{ex,MZ}$ , Fraction of LDOC of total microzoo. DOC excretion	0.75		-3.55	
$r^B_{MZ}$ , Microzoo. basal respiration rate, d <sup>-1</sup>	0.01		-3.32E-02	
$r^A_{MZ}$ , Microzoo. active respiration rate, d <sup>-1</sup>	0.30		-2.27	
$exADJ_{MZ}$ , Microzoo. extra SDOM excretion rate, d <sup>-1</sup>	2.0		0	
$remi_{MZ}$ , Microzoo. nutrient regeneration rate, d <sup>-1</sup>	4.68		-8.26E-02	
$pom_{MZ}$ , POM production rate per microzoo. gross growth, d <sup>-1</sup>	0.03		-0.18	
$\mu_{KR}$ , Maximum krill C-specific growth rate, d <sup>-1</sup>	0.7	1.46	-11.8	OP
$g_{MZ}$ , Microzoo. half-saturation concentration in krill grazing, mmol C m <sup>-3</sup>	0.5	0.79	0.761	CS
$ex_{KR}$ , Total DOM excretion rate per krill gross growth, d <sup>-1</sup>	0.1		2.34	
$f_{ex,KR}$ , Fraction of labile DOC of total krill DOC excretion	0.25		-0.61	
$r^B_{KR}$ , Krill basal respiration rate, d <sup>-1</sup>	0.03		0.133	
$r^A_{KR}$ , Krill active respiration rate, d <sup>-1</sup>	0.09		0.309	
$exADJ_{KR}$ , Krill extra SDOM excretion rate, d <sup>-1</sup>	2.0		0	
$remi_{KR}$ , Krill nutrient regeneration rate, d <sup>-1</sup>	4.0		-0.383	
$pom_{KR}$ , POM production rate per krill gross growth, d <sup>-1</sup>	0.15		1.42	
$exREFR_{KR}$ , Krill RDOC production rate, d <sup>-1</sup>	0.02		0.108	
$remv_{KR}$ , Krill removal rate by higher-trophic levels, (mmol C m <sup>-3</sup> ) <sup>-1</sup> d <sup>-1</sup>	0.05	0.04	4.41	OP
$f_{KR}$ , Fraction of SDOM production by krill	0.1		0.889	
$f_{POM,HZ}$ , Fraction of POM production by higher-trophic level	0.2		2.15	
$exREFRSDOM$ , Conversion rate of SDOM to RDOM, d <sup>-1</sup>	0.0009		2.67E-03	
$q^C_{N,RDOM}$ , RDOM N/C ratio, mol N (mol C) <sup>-1</sup>	0.05		2.43E-02	
$q^C_{P,RDOM}$ , RDOM P/C ratio, mol P (mol C) <sup>-1</sup>	0.00065		3.68E-02	
$q^C_{N,POM}$ , N/C ratio for POM production by microzoo. and krill, mol N (mol C) <sup>-1</sup>	0.12		0.162	
$q^C_{P,POM}$ , P/C ratio for POM production by microzoo. and krill, mol P (mol C) <sup>-1</sup>	0.00045		0.967	
$r_{nitr}$ , Nitrification rate (NH <sub>4</sub> to NO <sub>3</sub> ), d <sup>-1</sup>	0.076		-0.25	
$prf_N$ , Preference for dissolving N content in POM	1.1		-1.73E-03	
$prf_P$ , Preference for dissolving P content in POM	4.0		-2.42E-02	
$wnsv$ , Detritus vertical sinking velocity, m d <sup>-1</sup>	6.0		4.70E-02	
$diss$ , Detrital dissolution rate, d <sup>-1</sup>	0.01		-5.23E-02	

**Table S5**

Model parameter	Init.	Opt.	Gradient	Mark
$A_E$ , Arrhenius parameter for temperature function	4000		9	
$\mu_{DA}$ , Diatom C-specific maximum growth rate, $d^{-1}$	2.0	2.13	-0.128	OP
$\mu_{CR}$ , Crypto. C-specific maximum growth rate, $d^{-1}$	1.0		-3.62	
$a_{DA}$ , Initial slope of P-I curve of diatoms, mol C (g Chl) $^{-1}$ $d^{-1}$ ( $W\ m^{-2}$ ) $^{-1}$	0.65	1.78	-18.4	OP
$a_{CR}$ , Initial slope of P-I curve of crypto., mol C (g Chl) $^{-1}$ $d^{-1}$ ( $W\ m^{-2}$ ) $^{-1}$	0.35		-5.29	
$\beta_{DA}$ , Light inhibition parameter for diatom photosynthesis ( $W\ m^{-2}$ ) $^{-1}$	0.005		1.87	
$\beta_{CR}$ , Light inhibition parameter for crypto. photosynthesis ( $W\ m^{-2}$ ) $^{-1}$	0.005		0.648	
$v^N_{REF,DA}$ , Maximum N uptake rate per diatom C biomass, mol N (mol C) $^{-1}$ $d^{-1}$	0.5		-1.79	
$v^N_{REF,CR}$ , Maximum N uptake rate per crypto. C biomass, mol N (mol C) $^{-1}$ $d^{-1}$	0.3		-0.21	
$k^{NH4}_{DA}$ , NH <sub>4</sub> half-saturation concentration for diatom uptake, mmol m $^{-3}$	0.1		-3.08	
$k^{NH4}_{CR}$ , NH <sub>4</sub> half-saturation concentration for crypto. uptake, mmol m $^{-3}$	0.1		-0.153	
$k^{NO3}_{DA}$ , NO <sub>3</sub> half-saturation concentration for diatom uptake, mmol m $^{-3}$	0.9		3.14	
$k^{NO3}_{CR}$ , NO <sub>3</sub> half-saturation concentration for crypto. uptake, mmol m $^{-3}$	0.6		0.159	
$v^P_{REF,DA}$ , Maximum P uptake rate per diatom C biomass, mol P (mol C) $^{-1}$ $d^{-1}$	0.02		8.77	
$v^P_{REF,CR}$ , Maximum P uptake rate per crypto. C biomass, mol P (mol C) $^{-1}$ $d^{-1}$	0.02		0.337	
$k^{PO4}_{DA}$ , PO <sub>4</sub> half-saturation concentration for diatom uptake, mmol m $^{-3}$	0.05		-0.392	
$k^{PO4}_{CR}$ , PO <sub>4</sub> half-saturation concentration for crypto. uptake, mmol m $^{-3}$	0.04		-1.23E-02	
$\zeta^{NO3}$ , C requirement (respiration) to assimilate NO <sub>3</sub> , mol C (mol N) $^{-1}$	0.1		1.72	
$\Theta$ , Maximum Chl/N ratio, g Chl <i>a</i> (mol N) $^{-1}$	1.5	3.04	-1.28E-07	CS
$expSV,DA$ , Diatom passive excretion rate per biomass, $d^{-1}$	0.00005		3.06E-02	
$expSV,CR$ , Crypto. passive excretion rate per biomass, $d^{-1}$	0.00005		1.14E-03	
$exact,DA$ , Diatom active excretion rate per growth rate, $d^{-1}$	0.00005		-8.21E-03	
$exact,CR$ , Crypto. active excretion rate per growth rate, $d^{-1}$	0.00005		-2.62E-04	
$pom_{DA}$ , POM production rate by diatom aggregation, (mmol C m $^{-3}$ ) $^{-1}$ $d^{-1}$	0.02		2.13	
$pom_{CR}$ , POM production rate by crypto. aggregation, (mmol C m $^{-3}$ ) $^{-1}$ $d^{-1}$	0.02		0.848	
$k^{DOC,HNA}$ , DOC half-saturation concentration for HNA bacterial uptake, mmol C m $^{-3}$	0.5		-0.183	
$k^{DOC,LNA}$ , DOC half-saturation concentration for LNA bacterial uptake, mmol C m $^{-3}$	0.2		8.50E-02	
$r_{SDOC}$ , Parameter controlling SDOC lability	0.005		-1.58	
$\mu_{HNA}$ , Maximum HNA bacterial growth rate, $d^{-1}$	2.0	1.96	1.81E-07	CS
$\mu_{LNA}$ , Maximum LNA bacterial growth rate, $d^{-1}$	1.0	0.36	-1.79E-07	CS
$b_{RHNA}$ , Parameter control HNA bacterial active respiration rate versus production, (mmol C m $^{-3}$ $d^{-1}$ ) $^{-1}$	0.08		-4.28E-02	
$b_{RLNA}$ , Parameter control LNA bacterial active respiration rate versus production, (mmol C m $^{-3}$ $d^{-1}$ ) $^{-1}$	0.2		-2.16E-03	
$exADJ,HNA$ , HNA bacterial extra SDOC excretion rate, $d^{-1}$	2.0		0	
$exADJ,LNA$ , LNA bacterial extra SDOC excretion rate, $d^{-1}$	2.0		0	
$remiHNA$ , HNA bacterial nutrient regeneration rate, $d^{-1}$	8.0		-1.71	
$remiLNA$ , LNA bacterial nutrient regeneration rate, $d^{-1}$	2.0		-1.9	
$exREFR,HNA$ , HNA bacterial RDOC production rate, $d^{-1}$	0.04		0.535	
$exREFR,LNA$ , LNA bacterial RDOC production rate, $d^{-1}$	0.01		6.72E-02	
$f_{S,HNA}$ , HNA bacterial selection strength on SDOM	0.1		-1.82E-02	
$f_{S,LNA}$ , LNA bacterial selection strength on SDOM	0.7		-4.52E-02	
$r^B_{HNA}$ , HNA bacterial basal respiration rate, $d^{-1}$	0.04		0.381	
$r^B_{LNA}$ , LNA bacterial basal respiration rate, $d^{-1}$	0.01		0.104	
$r^A_{min,HNA}$ , HNA bacterial minimum active respiration rate, $d^{-1}$	0.08		2.56E-02	
$r^A_{min,LNA}$ , LNA bacterial minimum active respiration rate, $d^{-1}$	0.04		1.45E-03	
$r^A_{max,HNA}$ , HNA bacterial maximum active respiration rate, $d^{-1}$	0.4	0.21	2.47	OP
$r^A_{max,LNA}$ , LNA bacterial maximum active respiration rate, $d^{-1}$	0.1		0.277	
$morth_{HNA}$ , HNA bacterial mortality rate, $d^{-1}$	0.2		0.135	
$morth_{LNA}$ , LNA bacterial mortality rate, $d^{-1}$	0.01		8.84E-02	
$\mu_{MZ}$ , Microzoo. C-specific maximum growth rate, $d^{-1}$	1.2		2.72	
$g_{DA}$ , Diatom half-saturation concentration in microzoo. grazing, mmol C m $^{-3}$	1.0		0.502	
$g'_{DA}$ , Diatom half-saturation concentration in krill grazing, mmol C m $^{-3}$	1.0		7.36	

$g_{CR}$ , Crypto. half-saturation concentration in microzoo. grazing, mmol C m <sup>-3</sup>	1.0	0.12	-1.88E-07	CS
$g_{HNA}$ , HNA bacterial half-saturation concentration in microzoo. grazing, mmol C m <sup>-3</sup>	0.55	0.150	6.17E-08	CS
$g_{LNA}$ , LNA bacterial half-saturation concentration in microzoo. grazing, mmol C m <sup>-3</sup>	0.55	0.151	-1.40E-07	CS
$ex_{MZ}$ , Total DOM excretion rate per microzoo. gross growth, d <sup>-1</sup>	0.25		-1.62E-02	
$f_{ex,MZ}$ , Fraction of LDOC of total microzoo. DOC excretion	0.75		-2.15	
$r^B_{MZ}$ , Microzoo. basal respiration rate, d <sup>-1</sup>	0.01		-6.55E-02	
$r^A_{MZ}$ , Microzoo. active respiration rate, d <sup>-1</sup>	0.30		-0.724	
$exADJ_{MZ}$ , Microzoo. extra SDOM excretion rate, d <sup>-1</sup>	2.0		0	
$remi_{MZ}$ , Microzoo. nutrient regeneration rate, d <sup>-1</sup>	4.5		-9.73E-02	
$pom_{MZ}$ , POM production rate per microzoo. gross growth, d <sup>-1</sup>	0.03		-8.71E-02	
$\mu_{KR}$ , Maximum krill C-specific growth rate, d <sup>-1</sup>	0.7	0.7	-19.3	OP
$g_{MZ}$ , Microzoo. half-saturation concentration in krill grazing, mmol C m <sup>-3</sup>	0.5	0.5	-0.299	OP
$ex_{KR}$ , Total DOM excretion rate per krill gross growth, d <sup>-1</sup>	0.3		-1.18	
$f_{ex,KR}$ , Fraction of labile DOC of total krill DOC excretion	0.25		-6.09	
$r^B_{KR}$ , Krill basal respiration rate, d <sup>-1</sup>	0.03		0.397	
$r^A_{KR}$ , Krill active respiration rate, d <sup>-1</sup>	0.09		1.08	
$exADJ_{KR}$ , Krill extra SDOM excretion rate, d <sup>-1</sup>	2.0		5.35E-02	
$remi_{KR}$ , Krill nutrient regeneration rate, d <sup>-1</sup>	4.0		-1.15	
$pom_{KR}$ , POM production rate per krill gross growth, d <sup>-1</sup>	0.10		0.943	
$exREFR_{KR}$ , Krill RDOC production rate, d <sup>-1</sup>	0.02		4.64E-02	
$remv_{KR}$ , Krill removal rate by higher-trophic levels, (mmol C m <sup>-3</sup> ) <sup>-1</sup> d <sup>-1</sup>	0.05	0.04	8.12	OP
$f_{KR}$ , Fraction of SDOM production by krill	0.1		-0.472	
$f_{POM,HZ}$ , Fraction of POM production by higher-trophic level	0.2		-0.724	
$exREFRSDOM$ , Conversion rate of SDOM to RDOM, d <sup>-1</sup>	0.0009		1.06E-03	
$q^C_{N,RDOM}$ , RDOM N/C ratio, mol N (mol C) <sup>-1</sup>	0.05		-0.418	
$q^C_{P,RDOM}$ , RDOM P/C ratio, mol P (mol C) <sup>-1</sup>	0.00065		0.13	
$q^C_{N,POM}$ , N/C ratio for POM production by microzoo. and krill, mol N (mol C) <sup>-1</sup>	0.12		-3.51	
$q^C_{P,POM}$ , P/C ratio for POM production by microzoo. and krill, mol P (mol C) <sup>-1</sup>	0.00045		3.24	
$r_{nitr}$ , Nitrification rate (NH <sub>4</sub> to NO <sub>3</sub> ), d <sup>-1</sup>	0.076		3.09	
$prf_N$ , Preference for dissolving N content in POM	1.1		2.20E-02	
$prf_P$ , Preference for dissolving P content in POM	4.0		-9.51E-02	
$wnsv$ , Detritus vertical sinking velocity, m d <sup>-1</sup>	6.0		9.37E-02	
$diss$ , Detrital dissolution rate, d <sup>-1</sup>	0.01		-0.112	

**Table S6**

Climatological model					
Model parameter		Init.	Opt.	Gradient	Mark
$A_E$ , Arrhenius parameter for temperature function	4000		-5.14		
$\mu_{DA}$ , Diatom C-specific maximum growth rate, $d^{-1}$	2.0		10.7		
$\mu_{CR}$ , Crypto. C-specific maximum growth rate, $d^{-1}$	1.0		0.882		
$a_{DA}$ , Initial slope of P-I curve of diatoms, mol C (g Chl) $^{-1}$ $d^{-1}$ ( $W m^{-2}$ ) $^{-1}$	0.65	1.46	1.13E-07	CS	
$a_{CR}$ , Initial slope of P-I curve of crypto., mol C (g Chl) $^{-1}$ $d^{-1}$ ( $W m^{-2}$ ) $^{-1}$	0.35		0.512		
$\beta_{DA}$ , Light inhibition parameter for diatom photosynthesis ( $W m^{-2}$ ) $^{-1}$	0.005		-1.08		
$\beta_{CR}$ , Light inhibition parameter for crypto. photosynthesis ( $W m^{-2}$ ) $^{-1}$	0.005		-6.41E-02		
$v^N_{REF,DA}$ , Maximum N uptake rate per diatom C biomass, mol N (mol C) $^{-1}$ $d^{-1}$	0.5		-0.251		
$v^N_{REF,CR}$ , Maximum N uptake rate per crypto. C biomass, mol N (mol C) $^{-1}$ $d^{-1}$	0.3		4.86E-03		
$k^{NH4}_{DA}$ , NH <sub>4</sub> half-saturation concentration for diatom uptake, mmol m $^{-3}$	0.1		-0.456		
$k^{NH4}_{CR}$ , NH <sub>4</sub> half-saturation concentration for crypto. uptake, mmol m $^{-3}$	0.1		-2.33E-02		
$k^{NO3}_{DA}$ , NO <sub>3</sub> half-saturation concentration for diatom uptake, mmol m $^{-3}$	0.9		0.465		
$k^{NO3}_{CR}$ , NO <sub>3</sub> half-saturation concentration for crypto. uptake, mmol m $^{-3}$	0.6		2.33E-02		
$v^P_{REF,DA}$ , Maximum P uptake rate per diatom C biomass, mol P (mol C) $^{-1}$ $d^{-1}$	0.03		2.75		
$v^P_{REF,CR}$ , Maximum P uptake rate per crypto. C biomass, mol P (mol C) $^{-1}$ $d^{-1}$	0.03		9.52E-02		
$k^{PO4}_{DA}$ , PO <sub>4</sub> half-saturation concentration for diatom uptake, mmol m $^{-3}$	0.05		-0.111		
$k^{PO4}_{CR}$ , PO <sub>4</sub> half-saturation concentration for crypto. uptake, mmol m $^{-3}$	0.04		-3.12E-03		
$\zeta^{NO3}$ , C requirement (respiration) to assimilate NO <sub>3</sub> , mol C (mol N) $^{-1}$	0.1		0.18		
$\Theta$ , Maximum Chl/N ratio, g Chl <i>a</i> (mol N) $^{-1}$	1.5	4.01	-9.94	OP	
$expSV,DA$ , Diatom passive excretion rate per biomass, $d^{-1}$	0.00005		1.22E-02		
$expSV,CR$ , Crypto. passive excretion rate per biomass, $d^{-1}$	0.00005		1.41E-03		
$exact,DA$ , Diatom active excretion rate per growth rate, $d^{-1}$	0.00005		-1.93E-03		
$exact,CR$ , Crypto. active excretion rate per growth rate, $d^{-1}$	0.00005		2.49E-05		
$pom_{DA}$ , POM production rate by diatom aggregation, (mmol C m $^{-3}$ ) $^{-1}$ $d^{-1}$	0.03		1.41		
$pom_{CR}$ , POM production rate by crypto. aggregation, (mmol C m $^{-3}$ ) $^{-1}$ $d^{-1}$	0.03		-2.77E-02		
$k^{DOC,HNA}$ , DOC half-saturation concentration for HNA bacterial uptake, mmol C m $^{-3}$	0.5		-0.138		
$k^{DOC,LNA}$ , DOC half-saturation concentration for LNA bacterial uptake, mmol C m $^{-3}$	0.2		-0.19		
$r_{SDOC}$ , Parameter controlling SDOC lability	0.005		0.21		
$\mu_{HNA}$ , Maximum HNA bacterial growth rate, $d^{-1}$	2.0	2.93	1.20E-07	CS	
$\mu_{LNA}$ , Maximum LNA bacterial growth rate, $d^{-1}$	1.0	0.16	2.70E-08	CS	
$b_{RHNA}$ , Parameter control HNA bacterial active respiration rate versus production, (mmol C m $^{-3}$ $d^{-1}$ ) $^{-1}$	0.08		1.16E-02		
$b_{RLNA}$ , Parameter control LNA bacterial active respiration rate versus production, (mmol C m $^{-3}$ $d^{-1}$ ) $^{-1}$	0.2		-1.76E-04		
$exADJ,HNA$ , HNA bacterial extra SDOC excretion rate, $d^{-1}$	2.0		0		
$exADJ,LNA$ , LNA bacterial extra SDOC excretion rate, $d^{-1}$	2.0		0		
$remiHNA$ , HNA bacterial nutrient regeneration rate, $d^{-1}$	8.0		-1.15		
$remiLNA$ , LNA bacterial nutrient regeneration rate, $d^{-1}$	2.0		-0.684		
$exREFR,HNA$ , HNA bacterial RDOC production rate, $d^{-1}$	0.04		-0.381		
$exREFR,LNA$ , LNA bacterial RDOC production rate, $d^{-1}$	0.01		-5.00E-02		
$f_{S,HNA}$ , HNA bacterial selection strength on SDOM	0.1		-1.25E-02		
$f_{S,LNA}$ , LNA bacterial selection strength on SDOM	0.7		-1.90E-02		
$r^B_{HNA}$ , HNA bacterial basal respiration rate, $d^{-1}$	0.04		-7.27E-02		
$r^B_{LNA}$ , LNA bacterial basal respiration rate, $d^{-1}$	0.01		2.41E-02		
$r^A_{min,HNA}$ , HNA bacterial minimum active respiration rate, $d^{-1}$	0.08		-4.40E-03		
$r^A_{min,LNA}$ , LNA bacterial minimum active respiration rate, $d^{-1}$	0.04		1.17E-04		
$r^A_{max,HNA}$ , HNA bacterial maximum active respiration rate, $d^{-1}$	0.4	0.29	3.30E-07	OP	
$r^A_{max,LNA}$ , LNA bacterial maximum active respiration rate, $d^{-1}$	0.1		6.64E-02		
$morth_{HNA}$ , HNA bacterial mortality rate, $d^{-1}$	0.2		-0.674		
$morth_{LNA}$ , LNA bacterial mortality rate, $d^{-1}$	0.01		-1.97E-02		
$\mu_{MZ}$ , Microzoo. C-specific maximum growth rate, $d^{-1}$	2.5		-2.83		
$g_{DA}$ , Diatom half-saturation concentration in microzoo. grazing, mmol C m $^{-3}$	1.0		-0.242		
$g_{DA}$ , Diatom half-saturation concentration in krill grazing, mmol C m $^{-3}$	1.0	0.75	6.27E-08	CS	

$g_{CR}$ , Crypto. half-saturation concentration in microzoo. grazing, mmol C m <sup>-3</sup>	1.0	0.09	-4.93E-08	CS
$g_{HNA}$ , HNA bacterial half-saturation concentration in microzoo. grazing, mmol C m <sup>-3</sup>	0.55	0.11	2.00E-07	CS
$g_{LNA}$ , LNA bacterial half-saturation concentration in microzoo. grazing, mmol C m <sup>-3</sup>	0.55		0.313	
$ex_{MZ}$ , Total DOM excretion rate per microzoo. gross growth, d <sup>-1</sup>	0.15		0.832	
$f_{ex,MZ}$ , Fraction of LDOC of total microzoo. DOC excretion	0.75		-1.43	
$r^B_{MZ}$ , Microzoo. basal respiration rate, d <sup>-1</sup>	0.01		2.64E-02	
$r^A_{MZ}$ , Microzoo. active respiration rate, d <sup>-1</sup>	0.30		0.614	
$exADJ_{MZ}$ , Microzoo. extra SDOM excretion rate, d <sup>-1</sup>	2.0		0	
$remi_{MZ}$ , Microzoo. nutrient regeneration rate, d <sup>-1</sup>	4.68		-0.104	
$pom_{MZ}$ , POM production rate per microzoo. gross growth, d <sup>-1</sup>	0.03		9.84E-02	
$\mu_{KR}$ , Maximum krill C-specific growth rate, d <sup>-1</sup>	0.7		-3.57	
$g_{MZ}$ , Microzoo. half-saturation concentration in krill grazing, mmol C m <sup>-3</sup>	0.5		-2.95	
$ex_{KR}$ , Total DOM excretion rate per krill gross growth, d <sup>-1</sup>	0.1		1.77	
$f_{ex,KR}$ , Fraction of labile DOC of total krill DOC excretion	0.25		-1.7	
$r^B_{KR}$ , Krill basal respiration rate, d <sup>-1</sup>	0.03		-0.264	
$r^A_{KR}$ , Krill active respiration rate, d <sup>-1</sup>	0.09		-0.315	
$exADJ_{KR}$ , Krill extra SDOM excretion rate, d <sup>-1</sup>	2.0		0	
$remi_{KR}$ , Krill nutrient regeneration rate, d <sup>-1</sup>	4.0		-0.305	
$pom_{KR}$ , POM production rate per krill gross growth, d <sup>-1</sup>	0.15		1.11	
$exREFR_{KR}$ , Krill RDOC production rate, d <sup>-1</sup>	0.02		-8.11E-02	
$remv_{KR}$ , Krill removal rate by higher-trophic levels, (mmol C m <sup>-3</sup> ) <sup>-1</sup> d <sup>-1</sup>	0.05	0.07	-0.264	OP
$f_{KR}$ , Fraction of SDOM production by krill	0.1		0.895	
$f_{POM,HZ}$ , Fraction of POM production by higher-trophic level	0.2		1.96	
$exREFRSDOM$ , Conversion rate of SDOM to RDOM, d <sup>-1</sup>	0.0009		-1.65E-02	
$q^C_{N,RDOM}$ , RDOM N/C ratio, mol N (mol C) <sup>-1</sup>	0.05		-0.11	
$q^C_{P,RDOM}$ , RDOM P/C ratio, mol P (mol C) <sup>-1</sup>	0.00065		5.75E-02	
$q^C_{N,POM}$ , N/C ratio for POM production by microzoo. and krill, mol N (mol C) <sup>-1</sup>	0.12		0.424	
$q^C_{P,POM}$ , P/C ratio for POM production by microzoo. and krill, mol P (mol C) <sup>-1</sup>	0.00045		1.42	
$r_{nitr}$ , Nitrification rate (NH <sub>4</sub> to NO <sub>3</sub> ), d <sup>-1</sup>	0.076		0.493	
$prf_N$ , Preference for dissolving N content in POM	1.1		-9.55E-02	
$prf_P$ , Preference for dissolving P content in POM	4.0		-2.44E-02	
$wnsv$ , Detritus vertical sinking velocity, m d <sup>-1</sup>	6.0		-2.27	
$diss$ , Detrital dissolution rate, d <sup>-1</sup>	0.01		-3.05E-02	

**Table S7**

Unit: mmol m <sup>-3</sup> mmol m <sup>-3</sup> d <sup>-1</sup>	2010-11: +T anomaly, -ice anomaly 0.11 ± 0.89°C, 9 ± 18%		2011-12: -T anomaly, +ice anomaly -0.13 ± 0.83°C, 24 ± 38%		2012-13: +T anomaly, -ice anomaly 0.04 ± 1.00°C, 13 ± 22%		2013-14: +T anomaly, +ice anomaly 0.09 ± 0.52°C, 38 ± 37%	
	Maximum	Mean ± S.D.	Maximum	Mean ± S.D.	Maximum	Mean ± S.D.	Maximum	Mean ± S.D.
BP, obs (mod)	0.44 (0.12)	0.11 ± 0.09 (0.07 ± 0.02)	0.19 (0.31)	0.04 ± 0.04 (0.16 ± 0.08)	1.57 (0.30)	0.10 ± 0.15 (0.17 ± 0.08)	0.38 (0.09)	0.12 ± 0.10 (0.06 ± 0.02)
HNA, obs (mod)	0.42 (0.23)	0.28 ± 0.10 (0.18 ± 0.04)	0.06 (0.95)	0.04 ± 0.02 (0.71 ± 0.23)	0.57 (0.75)	0.21 ± 0.17 (0.44 ± 0.18)	0.65 (0.20)	0.27 ± 0.20 (0.16 ± 0.04)
LNA, obs (mod)	0.49 (0.38)	0.38 ± 0.07 (0.31 ± 0.03)	0.83 (0.33)	0.34 ± 0.25 (0.32 ± 0.01)	0.34 (0.34)	0.18 ± 0.07 (0.32 ± 0.02)	0.65 (0.35)	0.38 ± 0.17 (0.33 ± 0.02)
DA, obs (mod)	16.4 (3.1)	3.00 ± 2.88 (1.43 ± 0.74)	-	-	34.2 (1.72)	3.48 ± 6.21 (1.02 ± 0.48)	20.1 (2.09)	2.00 ± 2.77 (1.11 ± 0.56)
CR, obs (mod)	0.57 (0.22)	0.12 ± 0.10 (0.15 ± 0.05)	-	-	2.78 (1.56)	0.44 ± 0.58 (0.61 ± 0.45)	7.58 (0.21)	0.60 ± 1.26 (0.15 ± 0.05)
PP, obs (mod)	92.8 (152.4)	17.9 ± 21.1 (19.5 ± 27.2)	70.7 (51.2)	13.0 ± 13.3 (17.2 ± 14.2)	627 (54.8)	89.3 ± 97.8 (18.0 ± 15.8)	959 (47.9)	157 ± 223 (13.2 ± 11.4)
POC, obs (mod)	29.4 (24.5)	9.63 ± 5.79 (12.1 ± 2.69)	49.1 (14.4)	13.3 ± 8.36 (11.7 ± 1.06)	-	-	-	-
SDOC, obs (mod)	53.7 (13.2)	12.4 ± 9.28 (10.8 ± 1.38)	37.4 (12.7)	8.05 ± 5.88 (10.8 ± 1.24)	-	-	-	-

## **Text S1. Model processes**

The model simulates biological-physical model processes for a 1-D vertical water column, solving numerically for a discretized version of the time-rate of change for each model state variable. The original model schemes are detailed in Kim et al. (2021). For a generic tracer variable  $C$  the time-rate of change equation takes the form (Glover et al. 2011):

$$\frac{\partial C}{\partial t} = -\frac{\partial}{\partial z} (wC) + \frac{\partial}{\partial z} \left( K_z \frac{\partial C}{\partial z} \right) + J_C \quad (\text{S1})$$

where  $z$  is the depth,  $w$  is the vertical velocity (the sum of water motion and gravitational particle sinking),  $K_z$  is the turbulent eddy diffusivity, and  $J_C$  is the biological and biogeochemical net source and sink term for  $C$ . The physical advection and mixing terms are applied sequentially following the computation of the biological and biogeochemical terms  $J_C$  using a constant time step  $dt$  of 1 hour. The contributions of the source/sink term  $J_C$  to the time rate of change equations are constructed as a series of coupled ordinary differential equations (Appendix in Kim et al. 2021) and solved using a second-order Runge-Kutta numerical integration scheme. The model simulates the dynamics of C, N, and P, but here we only focus on the presentation of the model C dynamics. The cellular molar (N/C or P/C) quota parameters of the most state variables are fixed and not submitted to the optimization and data assimilation procedure. To first order, a variety of the model physiological processes are affected by water temperature, including the maximum growth rates of phytoplankton, bacteria, and zooplankton and basal respiration rates of bacteria and zooplankton. The Arrhenius function is implemented to change these physiological rates as a function of water temperature. The net change of each stock is determined by its source and sink terms.

## **Text S2. Physical forcing**

The model is forced by mixed layer depth (MLD), photosynthetically active radiation (PAR) at the ocean surface, sea-ice concentration, water-column temperature, vertical velocity (set as zero; see Kim et al., 2021), and vertical eddy diffusivity, at a temporal resolution of 1 day. Temperature, sea ice, and vertical eddy diffusivity are set up at every depth point. How each of these forcing fields is calculated and set up for model grids are detailed in Kim et al (2021). The temporal evolution of the model state variables and flows is affected by physical derivatives from vertical advection, vertical diffusion, bottom boundary exchange, and sinking of detritus, which requires inputs of vertical velocity, vertical diffusive coefficient, MLD, and sinking speed of detritus. The model implements the mixing scheme where vertical advection and detrital sinking are demonstrated with a third-order direct space-time upwind-biased scheme (Hundsrfer & Trompert, 1994) and the Sweby flux limiter (Sweby, 1984) but simplified to work for 1-D vertical advection only. Vertical diffusion is applied using a Crank-Nicholson vertically variable diffusion operation (Press et al., 1986) with a closed upper boundary and an open bottom boundary.

## **Text S3. Data assimilation and parameter optimization processes**

The model utilizes a variational adjoint data assimilation scheme (Lawson et al., 1995) to the data-assimilation scheme (Fig. 2 in main text) consisting of four main steps (Glover et al., 2011). First, the model is integrated forward in time (i.e., forward model) from prescribed initial conditions and initial model parameter values (Tables S2-6) to calculate the model-observation misfits referred as total cost function or total cost. Second, an adjoint model constructed using the Tangent linear and Adjoint Model Compiler (TAPENADE) is integrated backward in time and compute the gradients of the total cost with respect to the model parameters. Third, the computed gradients are passed to a limited-memory quasi-Newton optimization software M1QN3 3.1 (Gilbert & Lemaréchal, 1989) to determine the direction and optimal step size by which the model parameters need to be modified to reduce the total cost. Finally, a new forward model simulation is performed using the new set of modified parameters from the third step. These four steps are conducted in an iterative manner until the pre-set convergence criteria are

satisfied ensuring the convergence of the optimized parameters and a local minimum achieved by the total cost, via low gradients (sensitivity) of the total cost with respect to each optimized parameter and positive eigenvalues of the Hessian matrix.

Initial values of the model parameters (a total of 84 free or optimizable parameters, Tables S2-6) are assigned based on literature values (Caron et al., 2000, Luo et al., 2010, Garzio et al., 2013). Optimization starts by submitting a subset of these 84 free model parameters rather than submitting all of them at once. The initial parameter subset submitted to optimization consists of 10 different model parameters, with one parameter per each state variable, the change of which yielded the largest decrease in the total cost function during preliminary sensitivity tests, including  $\alpha_{DA}$  (the initial slope of the photosynthesis versus irradiance curve of diatoms, mol C (g Chl  $a$ ) $^{-1}$  d $^{-1}$  (W m $^{-2}$ ) $^{-1}$ ),  $\alpha_{CR}$  (the initial slope of the photosynthesis versus irradiance curve of cryptophytes, mol C (g Chl  $a$ ) $^{-1}$  d $^{-1}$  (W m $^{-2}$ ) $^{-1}$ ),  $\Theta$  (the maximum Chl:N ratio, g Chl  $a$  (mol N) $^{-1}$ ),  $\mu_{HNA}$  (the maximum HNA growth rate, d $^{-1}$ ),  $r_{max,HNA}^A$  (the maximum HNA active respiration rate, d $^{-1}$ ),  $g_{HNA}$  (the half-saturation density of HNA bacteria in microzooplankton grazing, mmol C m $^{-3}$ ),  $\mu_{MZ}$  (the maximum microzooplankton growth rate, d $^{-1}$ ),  $\mu_{KR}$  (the maximum krill growth rate, d $^{-1}$ ), and  $remv_{KR}$  (the krill removal rate by higher-trophic levels, (mmol C m $^{-3}$ ) $^{-1}$  d $^{-1}$ ; Tables S2-6).

If the parameters are optimized to ecologically unrealistic values, they are kept back to their initial values and removed from the next optimization cycle. Optimized parameters with  $\alpha f$  larger than 50% are updated but removed from the next optimization cycle (i.e., defined as ‘optimized’ parameters, or ‘OP’, Tables S2-6, detailed in Section 2.5), while optimized parameters with  $\alpha f$  smaller than 50% are updated and kept for the next optimization cycle (i.e., defined as ‘constrained parameters’, or ‘CS’, Tables S2-6). Constrained parameters are reported with uncertainties, while optimized parameters are reported without uncertainties because both changed parameters consist of an optimized model parameter set, but the parameters reported with the uncertainty ranges are the ones optimized with relatively small uncertainties and considered constrained. Every assimilation cycle, we ensure that bacterial model parameters are optimized in the direction to properly represent the dynamics associated with each bacterial group (Table 1) where we assign different magnitudes of each parameter value based on the best guesses and literatures (del Giorgio & Cole, 1998; Jiao et al., 2010). For instance, the maximum HNA bacterial growth rate ( $\mu_{HNA}$ , d $^{-1}$ ) is assigned to be higher than the maximum LNA bacterial growth rate ( $\mu_{LNA}$ , d $^{-1}$ ) prior to optimization, and ensured to keep being optimized to be higher during optimization. If  $\mu_{HNA}$  is optimized smaller than  $\mu_{LNA}$ ,  $\mu_{HNA}$  is set back to its original value instead of being updated. This way, a part of the initial parameter subset forms a final optimized parameter set. The gradients of the total cost function with respect to all 84 parameters are then evaluated, the parameters with large gradients (e.g., ~10) are resubmitted to optimization to further reduce the total cost, the gradients are evaluated again, and these cycles repeat until the termination of optimization. Optimization terminates when the gradients are reasonably low (e.g., < 0.01 for constrained parameters, < 5 for optimized parameters, and < 10 for unoptimized parameters).

#### Text S4. Model initialization, spin-up, and boundary conditions

The model is initialized by prescribing initial conditions 150 days (June 1) prior to the model start date of the growth season (November 1). This 150-day spin up is conducted in order to minimize the impact of initial conditions on the model output over the Austral growth season (November - March). Initial conditions are prepared by first generating an optimized model simulation of the full annual cycle that is forced by climatological physics and assimilated with climatological observations (i.e., climatological year or climatological model; 2010-11, 2011-12, 2012-13, and 2013-14). To capture a non-linear aspect of the WAP ecosystem system dynamics (e.g., strong interannual variability in the phytoplankton bloom phenology), we construct the climatological year by applying a single time shift to all the variables so that a seasonal PP peak of each year lines up with an average date of seasonal PP peaks from all years. Next, the output from the climatological simulation for June 1 conditions following the end of the seasonal growth season is used as the Austral winter initial condition for 2010-11. The resulting simulated conditions for June 1, 2012 from the optimized 2011-12 model is then used as the initial conditions for the 2012-13 simulation, and so on.

Modelling 0, 10, and 20 m requires non-zero bottom boundary values from 20 m, because of high biological and biogeochemical activities there, but there are no available observations of HNA, LNA, microzooplankton, and krill carbon biomass, LDOC, detritus, and NH<sub>4</sub> at 20 m at the study site. Instead, we 1) estimate the climatological (2010-2013) HNA and LNA carbon biomass at 20 m using the ratio of bacterial production to group-specific carbon biomass observations at 10 and 20 m, 2) extract the climatological (2002-2011) modelled values of microzooplankton and krill carbon biomass, detritus, LDOC, and NH<sub>4</sub> at 20 m from the original WAP-1D-VAR v1.0 model (Kim et al., 2021), and 3) use the climatological (2010-2013) observations of diatom- and cryptophyte biomass at 20 m for their bottom boundary conditions.

### Text S5. Target error adjustment

In the original WAP-1D-VAR v1.0 model, we calculated the climatological mean and standard deviation of each variable in the mixed layer per observation (vertical profile) over an extended year period (2002-03 to 2011-12) to get a more generalized picture with large sample size, and used the climatological CV (from the same climatological mean and standard deviation) for target errors of the most data types and the same climatological standard deviation for target errors of the log-transformed data types. In other words, each data type was assigned with its own but non-time varying CV. In the present study though, MLD is mostly deeper than 10 m but frequently shallower than 20 m (Fig. S1), and following the way in Kim et al. (2021) would throw out most vertical profiles, decrease the sample size, and make inadequate cases for representing the overall observational errors and seasonal-interannual variations (e.g., for all data types the depth levels measured typically span surface, 10 m, 20 m, etc, so shallow MLD would leave vertical profiles with only one or at most two data points within the mixed layer). We instead calculate the climatological standard deviation, and CV in the upper 20 m (i.e., 0, 10, and 20 m) per profile over the 4 study years of our study, which we adjust to similar values in Kim et al. (2021) as they are, of course, higher than those in Kim et al. (2021), largely due to including the observations at 20 m when MLD is deeper than 20 m. For target error adjustment, we derive the ratios of the climatological CV (for most data types) and standard deviation (for the log-converted variables) between our study and Kim et al. (2021), average the ratio for the same categorical data types (e.g., nutrients (NO<sub>3</sub> and PO<sub>4</sub>), phytoplankton (diatoms, cryptophytes, and primary production), bacteria (HNA and LNA carbon biomass, and production), and multiply this ratio to what we calculate to reduce to the level in the “mixed layer” to avoid an overestimated target error of each data type. Though complicated, we choose to do this way of combining the target errors in Kim et al. (2021) and error adjustment, hoping that it would more realistically represent the dynamics at Palmer Station B and for the 4 study years in our study because the target errors in Kim et al. (2021) were calculated for the 11-year period of the data from the slightly offshore Palmer Station E.

### References

- Bertilsson, S., Berglund, O., Karl, D. M., & Chisholm, S. W. (2003). Elemental composition of marine Prochlorococcus and Synechococcus: Implications for the ecological stoichiometry of the sea. *Limnol. Oceanogr.* 48(5), 1721–1731.
- Caron, D. A., Dennett, M. R., Lonsdale, D. J., Moran, D. M., and Shalapyonok, L.: Microzooplankton herbivory in the Ross sea, Antarctica. *Deep-Sea Res. Pt. II*, 47, 3249–3272, 2000.
- del Giorgio, P. A., Cole, J. J. (1998) Bacterial growth efficiency in natural aquatic systems. *Annu. Rev. Ecol. Syst.* 29:503–541.
- Droop, M. R. (1974). The nutrient status of algal cells in continuous culture. *J. Mar. Biol. Assoc. U. K.*, 54(4), 825–855.
- Droop, M. R. (1983). 25 years of algal growth kinetics. A personal view. *Botanica Marina*.

- Friedrichs, M. A. M. (2002) Assimilation of JGOFS EqPac and SeaWiFS data into a marine ecosystem model of the central equatorial Pacific Ocean. *Deep Sea Res. II* 49:289–319.
- Friedrichs, M. A. M., Hood, R. R., Wiggert, J. D. (2006) Ecosystem model complexity versus physical forcing: quantification of their relative impact with assimilated Arabian Sea data. *Deep Sea Res. II* 53:576–600.
- Friedrichs, M. A. M., Dusenberry, J. A., Anderson, L. A., Armstrong, R. A. and others (2007) Assessment of skill and portability in regional marine biogeochemical models: role of multiple planktonic groups. *J. Geophys. Res.* 112:C08001.
- Garzio, L. M., Steinberg, D. K., Erickson, M., and Ducklow, H. W. (2013) Microzooplankton grazing along the Western Antarctic Peninsula. *Aquat. Microb. Ecol.*, 70, 215–232, <https://doi.org/10.3354/ame01655>.
- Geider, R. J., MacIntyre, H. L., & Kana, T. M. (1997). Dynamic model of phytoplankton growth and acclimation: Responses of the balanced growth rate and the chlorophyll a: carbon ratio to light, nutrient-limitation and temperature. *Mar. Ecol. Prog. Ser.*, 148(1/3), 187–200.
- Gilbert, J. C., and Lemaréchal, C. (1989). “Some Numerical Experiments with Variable-Storage Quasi-Newton Algorithms.” *Mathematical Programming* 45(1): 407–35.
- Glover, D. M., Jenkins, W. J., & Doney, S. C. (2011). 10. Model analysis and optimization. In *Modeling Methods for Marine Science*. Cambridge University Press.
- Jiao, Nianzhi et al. 2010. “Microbial Production of Recalcitrant Dissolved Organic Matter: Long-Term Carbon Storage in the Global Ocean.” *Nature Reviews Microbiology* 8(8): 593–99.
- Hundsdorfer W, Trompert RA (1994) Method of lines and direct discretization—a comparison for linear advection. *Appl. Numer. Math* 13:469–490
- Kirchman DL (1994) The uptake of inorganic nutrients by heterotrophic bacteria. *Microb. Ecol.* 28:255–271
- Kirchman DL (2000) Uptake and regeneration of inorganic nutrients by marine heterotrophic bacteria. In: Kirchman DL (ed)
- Kirk JTO (1994) Light and photosynthesis in aquatic systems. Cambridge University Press, New York, NY
- Klinck, J. M. (1998). Heat and salt changes on the continental shelf west of the Antarctic Peninsula between January 1993 and January 1994. *J. Geophys. Res.* 103(C4), 7617–7636.
- Matear RJ (1995) Parameter optimization and analysis of ecosystem models using simulated annealing: a case study at Station P. *J. Mar. Res.* 53:571–607
- McCarthy, J. (1980). *Nitrogen*. In: Morris I (ed) *The physiological ecology of phytoplankton*. Blackwell, Oxford.
- Montégut, C. de B., Madec, G., Fischer, A. S., Lazar, A., & Iudicone, D. (2004). Mixed layer depth over the global ocean: An examination of profile data and a profile-based climatology. *J. Geophys. Res.* 109(C12).
- Long, M. C., Lindsay, K., & Holland, M. M. (2015). Modeling photosynthesis in sea ice-covered waters. *Journal of Advances in Modeling Earth Systems*, 7(3), 1189-1206.

- Luo YW, Friedrichs MA, Doney SC, Church MJ, Ducklow HW (2010) Oceanic heterotrophic bacterial nutrition by semilabile DOM as revealed by data assimilative modeling. *Aquat. Microb. Ecol.* 60(3):273–287.
- Pinker RT, Laszlo I (1992) Global distribution of photosynthetically active radiation as observed from satellites. *J. Clim.* 5:56–65
- Press WH, Flannery BP, Teukolsky SA, Vetterling WT (1986) Numerical recipes: the art of scientific computing. Cambridge University Press, New York, NY
- Smith, D. A., Hofmann, E. E., Klinck, J. M., & Lascara, C. M. (1999). Hydrography and circulation of the West Antarctic Peninsula Continental Shelf. *Deep Sea Res. I*, 46(6), 925–949.
- Sweby PK (1984) High-resolution schemes using flux limiters for hyperbolic conservation-laws. *SIAM J Numer Anal* 21:995–1011
- Tziperman E, Thacker WC (1989) An optimal-control adjoint-equations approach to studying the oceanic general-circulation. *J. Phys. Oceanogr.* 19:1471–1485